# An Evaluation of Probes to Measure Oxidizing Organic Triplet Excited States in Aerosol Liquid

Lan Ma, Reed Worland†, Theo Tran, and Cort Anastasio\*

Water

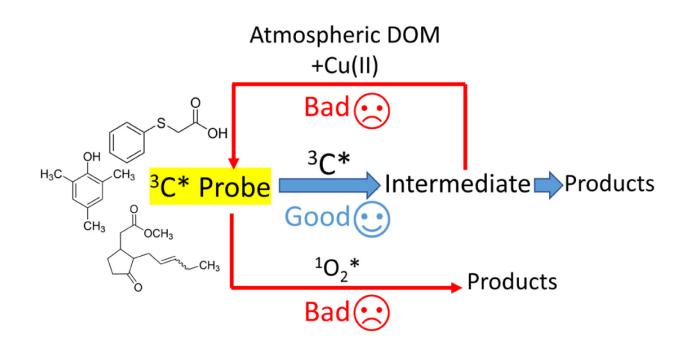
Department of Land, Air, and Water Resources, University of California, Davis, CA 95616

\*Correspondence to: Cort Anastasio (canastasio@ucdavis.edu)

Published in Environmental Science & Technology, 2022

https://doi.org/10.1021/acs.est.2c09672

# 1 For Table of Contents Only



#### **ABSTRACT**

5

Oxidizing triplet excited states of organic matter (3C\*) drive numerous reactions in fog/cloud drops and 6 7 aerosol liquid water (ALW). Quantifying oxidizing triplet concentrations in ALW is difficult because <sup>3</sup>C\* 8 probe loss can be inhibited by the high levels of dissolved organic matter (DOM) and copper in particle water, leading to an underestimate of triplet concentrations. In addition, illuminated ALW contains high 9 concentrations of singlet molecular oxygen ( ${}^{1}O_{2}^{*}$ ), which can interfere with  ${}^{3}C^{*}$  probes. Our overarching 10 goal is to find a triplet probe that has low inhibition by DOM and Cu(II), and low sensitivity to <sup>1</sup>O<sub>2</sub>\*. To 11 this end, we tested 12 potential probes from a variety of compound classes. Some probes are strongly 12 13 inhibited by DOM, while others react rapidly with <sup>1</sup>O<sub>2</sub>\*. One of the probe candidates, (phenylthiol)acetic acid (PTA), seems well suited for ALW conditions, with mild inhibition and fast rate constants with 14 15 triplets, but it also has weaknesses, including a pH-dependent reactivity. We evaluated the performance of 16 both PTA and syringol (SYR) as triplet probes in aqueous extracts of particulate matter extracts. While 17 PTA is less sensitive to inhibition than SYR, it results in lower triplet concentrations, possibly because it 18 is less reactive with weakly oxidizing triplets.

19

20

#### **KEYWORDS**

- 21 Photooxidants, dissolved organic matter, singlet molecular oxygen, particle water, aerosol liquid water,
- 22 inhibition factor

23

24

#### **SYNOPSIS**

- 25 Because current probes for oxidizing organic triplet excited states fare poorly in concentrated extracts of
- atmospheric particles, we evaluated a dozen molecules as possible alternatives.

### INTRODUCTION

29	Chromophoric dissolved organic matter (CDOM) in surface waters absorbs light to form triplet excited
30	states (3CDOM*), including an oxidizing subset (denoted as 3C*) that can react with numerous
31	environmental contaminants. 1-3 Oxidizing triplets are also important in atmospheric waters, e.g.,
32	cloud/fog drops and aerosol liquid water (ALW), where they react with organics to form aqueous
33	secondary organic aerosol (aqSOA), <sup>4-6</sup> and oxidize sulfite and organosulfur compounds to sulfate. <sup>7-9</sup>
34	Triplets also produce other oxidants, including hydroxyl radical (*OH), singlet molecular oxygen ( <sup>1</sup> O <sub>2</sub> *),
35	and hydrogen peroxide (HOOH). 10-13 While hydroxyl radical is generally the only oxidant considered in
36	models of fog/cloud chemistry, <sup>3</sup> C* can be equally important as a sink for certain organics since triplet
37	concentrations can be $10-100$ times higher than ${}^{\bullet}\mathrm{OH}.^{14,15}$ In addition, ${}^{3}\mathrm{C}^{*}$ concentrations are even higher
38	- by a few orders of magnitude - in ALW, where they appear to play a significant role in aqSOA
39	formation. 16,17 Therefore, knowing triplet steady-state concentrations is important to understand chemistry
40	in particle water. However, this goal is complicated since triplets represent a complex mixture with a wide
41	range of reactivities. <sup>1,18</sup>
42	There are two general types of probes for <sup>3</sup> CDOM* quantification: energy transfer and electron transfer.
43	The first type takes advantage of the fact that triplets with sufficient energy ( $E_T \ge 184 \text{ kJ mol}^{-1}$ ) can
44	transfer energy to dienes, resulting in their isomerization. 13,18-21 Monitoring the isomerization of a probe
45	like sorbic acid and its derivatives is commonly used to quantify <sup>3</sup> CDOM* concentrations. <sup>19,20</sup> The other
46	type of probe is electron transfer, where the oxidation of a probe such as 2,4,6-trimethylphenol (TMP) or
47	2,6-dimethoxyphenol (syringol or SYR) by <sup>3</sup> C* is monitored to determine the oxidizing triplet steady-
48	state concentration. 14,16,22,23 Since our long-term goal is to understand the contributions of triplets in
49	driving chemistry in particle water, our interest is on oxidizing triplets and so we focus here on electron-
50	transfer probes.
51	One complication with electron transfer probes is that DOM is both a photosensitizer that forms triplets,
52	but also an antioxidant that can inhibit triplet-induced oxidation. <sup>24–28</sup> For example, when compounds

containing phenol or aniline moieties react with a triplet, they donate an electron and form an intermediate phenoxyl or aniline radical, <sup>29</sup> which can be reduced by DOM to regenerate the parent compound. This inhibition of the decay of phenol/aniline probes by DOM leads to an underestimate of the triplet concentration. Similarly, nanomolar concentrations of Cu(II) inhibit the net decay of phenols and anilines by <sup>3</sup>C\*. <sup>17,30,31</sup>. While reactions of DOM and Cu(II) with oxidized products of phenols and anilines are environmentally relevant, they complicate accurate determination of triplet concentrations by probes and should be avoided or corrected. Another potential complication is the reaction of electron-poor phenoxyl radicals with phenol or aniline probes.<sup>32</sup> which could lead to an overestimate of <sup>3</sup>C\* concentrations, but we do not examine this issue here. An ideal electron-transfer triplet probe would be resistant to regeneration by DOM after oxidation and some electron-rich phenols like TMP are resistant to inhibition by DOM under surface water conditions (i.e., up to approximately 6 mg C L<sup>-1</sup> DOM). <sup>24,25,33,34</sup> N-cyclopropylanilines were developed as DOMregeneration-resistant triplet probes, where the oxidized intermediate undergoes rapid and irreversible ring-opening, avoiding reduction by aquatic DOM.<sup>35</sup> But it is unclear whether these probes work in concentrated aqueous extracts of particles. In addition to higher DOM levels (millimolar to several molar),  $^{36-40}$  aerosol liquid water has lower pH values ( $\leq 5$ ) $^{41-44}$  and much higher dissolved copper concentrations (up to several millimolar), 45-49 compared to surface waters. Additionally, biomass-burning influenced aerosols can contain high concentrations of phenols, potent antioxidants that increase probe inhibition. <sup>50–52</sup> In addition, since <sup>1</sup>O<sub>2</sub>\* concentrations can be higher than <sup>3</sup>C\* in ambient particle water, <sup>16</sup> a triplet probe for PM extracts should react quickly with <sup>3</sup>C\* but slowly with <sup>1</sup>O<sub>2</sub>\*. In this study we evaluate the suitability of 12 triplet probes under aqueous particle extract conditions. We examine the susceptibility of the probes for inhibition, including by a lab mixture of Cu(II) and syringol (a biomass-burning phenol) as well as by ambient particle extracts. To gauge the specificity of probes for triplets, we also measure the rate constants for each with singlet oxygen and a model atmospheric triplet. Based on our results, we identify a good candidate probe for triplets in atmospheric particle extracts and

53

54

55

56

57

58

59

60

61

62

63

64

65

66

67

68

69

70

71

72

73

74

75

76

compare its performance to syringol, a probe we have used in the past, in several illuminated particle extracts.

80

81

82

85

78

79

#### MATERIALS AND METHODS

#### Chemicals, Illuminations, and Kinetic Analysis

- Details on chemicals, illuminations, and the determination of first-order rate constants for probe loss
- 84  $(k'_{Light})$  are in Section S1 of the Supplemental Information.

#### Relative Rate Method

- We determined second-order rate constants of probe compounds with the triplet state of 3,4-
- dimethoxybenzaldehyde (DMB) at 20 °C using a relative rate method with methyl jasmonate (MeJA) as
- 88 the reference compound and simulated sunlight illumination.<sup>53</sup> For rate constants with singlet oxygen
- 89 (also at 20 °C), we used a relative rate method with furfuryl alcohol (FFA) as the reference and 549 nm
- 90 illumination. <sup>53–55</sup> Solutions containing 20 μM probe, 20 μM reference compound, and 100 μM DMB
- 91 (triplet precursor) or 20 μM Rose Bengal (<sup>1</sup>O<sub>2</sub>\* precursor) were prepared and adjusted to pH 4.2, a typical
- 92 value for ALW in California's Central Valley during winter. 42 We used 3DMB\* as our standard oxidizing
- 93 triplet because its reactivity appears similar to the average value of natural triplets in Davis fog waters and
- 94 PM extracts<sup>14,16</sup>. We took aliquots at certain reaction times to determine first-order decay rate constants of
- the reference  $(k'_{ref})$  and probe  $(k'_{probe})$ . The bimolecular rate constant of probe reacting with  ${}^{3}DMB^{*}$  or
- $^{1}O_{2}*(k_{probe+Ox})$  was then determined from

$$k_{probe+Ox} = \frac{k'_{probe}}{k'_{ref}} \times k_{ref+Ox}$$
 (1)

where  $k_{\text{ref+Ox}}$  is the second-order rate constant for the reference compound reacting with  ${}^{3}\text{DMB}^{*}$ 

99 
$$(k_{\text{MeJA+3DMB}*} = 4.1 (\pm 1) \times 10^8 \text{ M}^{-1} \text{ s}^{-1}) \text{ or } {}^{1}\text{O}_{2}* (k_{\text{FFA+1O2}*} = 0.96 (\pm 0.04) \times 10^8 \text{ M}^{-1} \text{ s}^{-1}).$$

#### **Inhibition Factors**

We quantified inhibition of triplet probe oxidation using: (1) aqueous particulate matter extracts (PME; see SI Section S2 for particle collection and extraction details), (2) Suwanee River Fulvic Acid, or (3) a mixture of SYR and CuSO<sub>4</sub> at a molar ratio of 70:1 ("SYR+Cu" solution) as a mimic of PME with high antioxidant activity. 10  $\mu$ M probe and a photosensitizer (15  $\mu$ M benzophenone (BP) or 80  $\mu$ M DMB) were spiked into either Milli-Q water, SYR+Cu solution, or PME, each adjusted to pH 4.2. Solutions were illuminated and the first-order rate constant of probe decay was determined. In our initial screening of probes we used BP, which forms a more reactive triplet than DMB<sup>1</sup>, so that experiments would be more rapid; later *IF* experiments used DMB, which is more relevant to atmospheric waters. The photodegradation of probe compound in PME or SYR+Cu solution without photosensitizer was also measured. The inhibition factor (*IF*<sub>P</sub>) for probe oxidation was calculated using<sup>24</sup>

$$IF_P = \frac{k'_{Sens,DOM} - k'_{DOM}}{k'_{Sens}} \tag{2}$$

where:  $k'_{Sens,DOM}$ ,  $k'_{DOM}$ , and  $k'_{Sens}$  are the first-order decay rate constants of probe loss in (1) a solution containing photosensitizer and either PME or SYR+Cu, in (2) PME or SYR+Cu solution without photosensitizer, and in (3) Milli-Q water containing photosensitizer, respectively.<sup>25</sup> All k' values were corrected for internal light screening due to absorption by PME or triplet photosensitizer with screening factors  $(S_{\lambda})$ , which were calculated with equation 2 in Smith et al.<sup>56</sup> For probe compounds that undergo direct photodegradation, we subtracted this contribution in the probe decay from all three k' terms. For compounds without direct photodegradation, the decay in SYR+Cu solution is zero (i.e.  $k'_{DOM} = 0$ ).

#### **Quantifying Oxidizing Triplet Excited States of Organic Matter in PM Extracts**

We determined concentrations of photogenerated  ${}^{\bullet}$ OH and  ${}^{1}$ O<sub>2</sub>\* in PME as described in SI Section S3 and Kaur et al.  ${}^{16}$  For oxidizing triplets, we spiked 10  $\mu$ M of triplet probe in PME, illuminated the solution, and measured the first-order decay rate constant  $k'_{P,exp}$ . These values were normalized to sunlight conditions at

midday on the winter solstice at Davis (solar zenith =  $62^{\circ}$ ;  $j_{2NB,win} = 0.0070 \text{ s}^{-1}$ ) and corrected for internal light screening:

$$k'_{P,norm} = \left[\frac{k'_{P,exp}}{S_{\lambda} \times j_{2NB,exp}}\right] \times j_{2NB,win}$$
 (3)

The contributions of \*OH and  ${}^{1}O_{2}$ \* to probe decay were subtracted from  $k'_{P,norm}$  to obtain  $k'_{P,3C*}$ , the first-order rate constant for probe loss due to triplets. We assume that  ${}^{3}C*$  in PME has the same average reactivity as  ${}^{3}DMB*$ ,  ${}^{16,57}$  so the  ${}^{3}C*$  concentration in a PME can be estimated with

$$[{}^{3}C^{*}]_{P} = \frac{k'_{P,3C^{*}}}{k_{P+3DMB^{*}}}$$
(4)

where  $k_{P+3DMB^*}$  is the second-order rate constant of probe with  $^3DMB^*$ . Rate constants for  $^3DMB^*$  with the probes at pH 4.2 are 3.9 ( $\pm$  0.7)  $\times$ 10<sup>9</sup> M<sup>-1</sup>s<sup>-1</sup> for SYR<sup>58</sup> and 2.5 ( $\pm$  0.6)  $\times$ 10<sup>9</sup> M<sup>-1</sup>s<sup>-1</sup> for PTA (Table S2). As discussed at the end of this paper, these  $^3DMB^*$ -probe rate constants might be higher than the corresponding values with natural triplets in the PM extracts. If this is the case, we are underestimating concentrations of oxidizing triplets. The triplet concentration in equation 4 is uncorrected for probe inhibition; as described below, this correction is included in equation 8.

#### **RESULTS AND DISCUSSION**

#### **Inhibition Effects on Triplet Probes in an Aerosol Water Mimic**

There are at least two ways in which DOM and other sample components can alter the oxidation of probes by triplet excited states: (1) regenerate the oxidized probe back to the parent form, which is an artifact that leads to an underestimate of the  ${}^{3}\text{C*}$  concentration, and (2) react directly with triplets to suppress their steady-state concentration, which is not an artifact but instead reflects what occurs in the environment. To quantify these two effects, we measure inhibition factors (*IF*, equation 2) in solutions containing a triplet precursor, triplet probe, and syringol and CuSO<sub>4</sub> as a lab mimic of particle water. SYR is a

surrogate for ALW phenols, which are one of the DOM groups that inhibit triplet-induced oxidation, <sup>26,60</sup> while Cu(II) is also present in atmospheric waters and inhibits the oxidation of phenols and anilines. <sup>30,31,46</sup> The *IF* quantifies how much SYR and Cu(II) inhibit net probe oxidation: a value of 1 indicates no inhibition, while an *IF* of 0 means that probe oxidation is fully suppressed. Since high concentrations of SYR can also suppress triplet concentrations, we also measure *IF* for furfuryl alcohol (FFA). FFA is a probe for singlet oxygen, <sup>61</sup> whose concentration will be proportional to the triplet concentration. <sup>1</sup> Therefore, FFA can be used to evaluate the extent of triplet suppression by DOM and other sample components. While Cu(II) can also quench <sup>3</sup>C\*, <sup>30</sup> the copper concentration is much lower than SYR, so Cu suppression of triplet concentrations in our *IF* experiments is negligible. To distinguish between triplet suppression and inhibition of probe oxidation, we define a corrected inhibition factor for the probe:

$$IF_{P,corr} = \frac{IF_P}{IF_{FFA}} \tag{5}$$

This corrected *IF*, which quantifies inhibition of probe oxidation by removing the influence of reduced triplet concentrations, is derived in SI Section S4.

We start by performing inhibition experiments with oxidizing triplet probes representing four different organic classes: 2,4,6-trimethyl phenol (TMP), methyl jasmonate (MeJA), *N*-cyclopropylaniline (CAN), and (phenylthio)acetic acid (PTA) (Figure 1). To examine the inhibition effect, we measure the pseudo first-order rate constants of probe decay by the triplet excited state of BP (<sup>3</sup>BP\*) in Milli-Q water and, separately, in SYR+Cu solution at pH 4.2. An example of the decays of TMP and MeJA in illuminated solution containing BP is in Figure S1.

Figure 1 shows the IF (Panel A) and  $IF_{P,corr}$  (Panel B) values for FFA and the four probes in the presence of 70  $\mu$ M SYR and 1  $\mu$ M Cu(II). The  $IF_{FFA}$  of 0.66 ( $\pm$  0.02) indicates that this concentration of syringol quenches roughly 34% of  $^3$ BP\* in air-saturated solutions. Assuming SYR has the same second-order rate constant with  $^3$ BP\* as does TMP (5 × 10 $^9$  M $^{-1}$  s $^{-1}$ ), $^{62}$  70  $\mu$ M SYR should quench 30% of  $^3$ BP\*, essentially the same as the measured IF, indicating that  $IF_{FFA}$  can quantify triplet suppression. As shown in Figure 1,

the  $IF_{MeJA}$  of 0.71 ( $\pm$  0.05) is not significantly different from  $IF_{FFA}$ , showing that MeJA oxidation by  ${}^{3}BP^{*}$ is not inhibited by SYR+Cu. This is also shown by the  $IF_{MeJA,corr}$  value of 1.08 ( $\pm$  0.08), which indicates IF<sub>P,corr</sub> describes inhibition of oxidation and not suppression of triplet concentration. Since oxidation of organic sulfur is not affected by phenol or natural organic matter, 8 sulfides such as (phenylthio)acetic acid might be robust triplet probes. The  $IF_{PTA,corr}$  value of 0.69 ( $\pm$  0.04) shows that PTA decay is mildly inhibited by SYR+Cu. <sup>3</sup>C\* oxidizes PTA to form a sulfur-centered radical cation, which undergoes rapid and irreversible decarboxylation, with a half-life of around 200 ns<sup>63,64</sup>. The resistance of PTA to inhibition is likely because the sulfur radical cation falls apart more quickly than it can be reduced to its parent compound. Both CAN and TMP show resistance to inhibition under surface water conditions. <sup>24,35</sup> However, in SYR+Cu solution their corrected IF values are smaller than 0.1, indicating that their oxidation by <sup>3</sup>BP\* is almost fully inhibited. In contrast, they are not inhibited by up to 20 mg C L<sup>-1</sup> of Suwannee River fulvic acid (SRFA), <sup>24,35</sup> indicating that our ALW mimic of SYR and Cu(II) is a more stringent test condition. Since Pan et al.<sup>30</sup> found that nanomolar concentrations of Cu(II) can decrease TMP decay, we also measured IF with SYR but not Cu(II). As shown in Figure S2,  $IF_{TMP,corr}$  with 70  $\mu$ M SYR is 0.51 ( $\pm$  0.04), indicating that syringol itself can inhibit TMP decay by <sup>3</sup>C\*, although not as significantly as Cu(II). This is consistent with the fact that SYR and TMP have similar redox potentials and so SYR can reduce the TMP phenoxyl radical cation back to TMP:  $E_{\rm OX}$  values vs. SHE are roughly 1.17 V for SYR (as measured for the SYR analog 3,4-dimethoxyphenol) and 1.22 V for TMP. 62,65-67 Since we use SYR as the mimic of atmospheric water DOM, we cannot examine  $IF_{SYR}$  with this mimic. Instead, we measure  $IF_{SYR}$  in a particle water extract (PME) with  ${}^{3}BP^{*}$ . As shown in Figure S3, we find that the corrected IF for methyl jasmonate in PME is not significantly different from 1, consistent with the result in Figure 1. In contrast,  $IF_{P,corr}$  values for SYR and TMP are 0.04 ( $\pm$  0.04) and 0.01 ( $\pm$  0.05), indicating that oxidation of SYR and TMP by <sup>3</sup>BP\* is strongly inhibited in particle extracts. Since TMP.

169

170

171

172

173

174

175

176

177

178

179

180

181

182

183

184

185

186

187

188

189

190

191

SYR, and CAN are strongly impacted by simulated ALW conditions, we search for a new triplet probe that is more resistant to inhibition.

195

196

197

198

199

200

201

202

203

204

205

206

207

208

209

210

211

212

213

214

215

216

193

194

#### **Screening Potential Triplet Probes**

An ideal triplet probe for aerosol liquid water would not be inhibited by DOM or Cu (i.e.,  $IF_{P,corr} \sim 1$ ) and would react rapidly with  ${}^{3}C^{*}$  but slowly with  ${}^{1}O_{2}^{*}$ . The rate constant with  ${}^{1}O_{2}^{*}$  is important because estimated <sup>1</sup>O<sub>2</sub>\* concentrations in ambient particle water are higher than those of oxidizing triplets. <sup>16</sup> We explored inhibition and singlet oxygen reactivity for 12 potential probes in five different organic classes: sulfides, alkenes, amines, phenols, and cyclopropylanilines. For each probe, we measured rate constants with <sup>1</sup>O<sub>2</sub>\* and <sup>3</sup>DMB\* at pH 4.2; we employ DMB as the triplet precursor because it is present in biomass-burning particles and its triplet state has a reactivity similar to ambient triplets in fog waters and particle water extracts. <sup>14,16,57</sup> We also calculated the fraction of probe reacting with <sup>3</sup>C\* in a concentrated PME (PM mass/liquid water mass ratio of  $4 \times 10^{-3}$  µg PM/µg H<sub>2</sub>O) to assess probe selectivity, using estimated  ${}^{\bullet}$ OH,  ${}^{3}$ C\*, and  ${}^{1}$ O<sub>2</sub>\* concentrations of 1.7 × 10<sup>-15</sup>, 4.1 × 10<sup>-13</sup>, and 8.5 × 10<sup>-12</sup> M, respectively.  ${}^{16}$ We measured the IF of each probe at pH 4.2 using <sup>3</sup>BP\* as the triplet and SYR+Cu as the mimic of reducing species in ALW. For compounds that absorb sunlight, we also measured direct photolysis rate constants. Structures for each probe are in Table S1, while Table 1 lists the results of our tests, which are summarized below. PTA reacts rapidly with the DMB triplet at pH 4.2 ( $k_{\text{PTA+3DMB}*} = 2.5 \times 10^9 \,\text{M}^{-1} \,\text{s}^{-1}$ ) and is significantly less reactive with  ${}^{1}O_{2}^{*}$ , with a rate constant ratio  $k_{\text{PTA+3DMB}^{*}}/k_{\text{PTA+1O2}^{*}}$  of 284 (± 71). At this high ratio,  ${}^{3}C^{*}$ account for 90% of PTA oxidation in PME, indicating the probe has good triplet selectivity. Though it undergoes direct photodegradation, this rate is negligible (roughly 50 times slower) compared with its decay rate by triplets in PME. Also, PTA shows only mild inhibition (described earlier), indicating it is a

promising probe. We also examined three PTA analogs, (phenylthio)acetyl chloride, 2-

217 (phenylthio)ethanol, and S-phenyl thioacetate. However, the first one rapidly hydrolyzes in water to form PTA, while the other two react slowly with  ${}^{3}DMB*$  ( $k < 10^{8} M^{-1} s^{-1}$ ) and 2-(phenylthiol)ethanol exhibits a 218 low IF value (0.14); because of its slow kinetics, we did not measure IF for S-phenyl thioacetate. 219 220 Alkenes appear to be a promising triplet probe class since methyl jasmonate (an alkene) shows very little 221 inhibition by DOM and SYR+Cu, as described above. However, four of the six alkenes we tested, including MeJA, have low values of  $k_{\text{probe+3DMB*}}/k_{\text{probe+1O2*}}$ , indicating relatively poor selectivity towards 222 <sup>3</sup>C\*. For the remaining two alkenes, other issues reduce their effectiveness as triplet probes. Terpineol 223 224 (TPN), like MeJA, has a corrected IF near one, indicating its decay is essentially not inhibited by 225 SYR+Cu, but it reacts relatively slowly with the DMB triplet (which was difficult to measure; see SI 226 Section S5) and thus has low specificity for triplets in particle water. Oxidation of the other alkene, 227 pulegone, is somewhat inhibited by SYR+Cu ( $IF_{P,corr} = 0.30$ ), which is not ideal but could work. 228 However, after performing our alkene probe tests we found in the literature that the reaction between alkenes and <sup>3</sup>C\* is not solely (or perhaps even predominantly) electron transfer, but also includes 229 photoaddition without electron transfer. <sup>68–70</sup> Because of this, alkenes do not necessarily solely capture 230 231 oxidizing triplets and might not be a suitable probe to quantify them; this might also explain why alkenes show only a modest correlation between rate constants with <sup>3</sup>BP\* and modeled one-electron oxidation 232 potentials.71 233 234 We next examined atenolol as a potential probe because some amines are resistant to regeneration by phenol after oxidation by  ${}^{3}\text{C}^{*}$  and show no inhibition by Cu(II).  ${}^{27,30}$  We measured  $IF_{\text{ANL.corr}}$  of 0.86 ( $\pm$ 235 0.05), indicating minor inhibition by SYR+Cu, but, its  ${}^{3}C^{*}/{}^{1}O_{2}^{*}$  rate constant ratio is low (55 (±16)), 236 237 indicating modest selectivity towards triplets in particle extracts. Our next class were the N-238 cyclopropylanilines, which were developed by Pflug et al. as triplet probes that are resistant to inhibition by SRFA at pH 7 and up to 20 mg C L<sup>-1</sup>. 35 However, in pH 4.2 solutions containing 70 μM SYR and 1 239 μM Cu(II), our two candidates - CAN and DCCAN - show low IF<sub>P,corr</sub> values (0.04 and 0.14, 240 respectively), indicating their decay by <sup>3</sup>BP\* is heavily inhibited. Moreover, the probes absorb sunlight 241

(290 – 310 nm) and undergo appreciable direct photodegradation in our studies; while Pflug et al. used UVA radiation (350 – 400 nm), our illumination system more closely simulates sunlight and includes wavelengths as low as 290 nm. <sup>15,35</sup> We also had difficulty determining the CAN rate constant with <sup>3</sup>DMB\*, obtaining a rate constant higher than 10<sup>10</sup> M<sup>-1</sup> s<sup>-1</sup>, the diffusion-controlled limit. This impossibly high value suggests there might be an unknown oxidant reacting with CAN in our illuminated solutions. Based on these results, CAN and DCCAN are poor choices for a <sup>3</sup>C\* probe under aerosol liquid water conditions. Lastly, the phenol probes (SYR and TMP) show strong inhibition by both PM extracts and SYR+Cu, as mentioned above, while TMP also has a modest <sup>3</sup>C\*/<sup>1</sup>O<sub>2</sub>\* rate constant ratio (Table 1).

#### **Kinetic Study on PTA**

Based on our results shown in Table 1, PTA appears to be the best choice for a triplet probe under particle extract conditions: it has a high  $k_{probe+3DMB^*}/k_{probe+102^*}$  ratio and is only mildly inhibited by syringol and Cu(II). Therefore, we further investigated PTA as a triplet probe. One disadvantage of PTA is that it is an acid, so its reactivity with triplets might vary with solution acidity. To explore this, we first determined the p $K_a$  of PTA based on light absorbance measurements, finding a value of 3.56 ( $\pm$  0.02) (Figure S5). To explore the pH dependence of PTA reactivity with  $^3DMB^*$ , we measured pseudo first-order rate constants of PTA decay with  $^3DMB^*$  at different pH (Figure 2). The decay rate of PTA peaks at pH 3.5, is roughly 5 times lower at pH 2 and 5, and approaches zero at pH values above 6. This trend is likely due to the different reactivities of the neutral and deprotonated forms of PTA. In addition, protonated  $^3DMB^*$  has a p $K_a$  value of 3.3, with the protonated form having generally higher reactivity with phenols. The measured first-order rate constant  $k'_{PTA}$  is the mole-fraction weighted reactivity of the protonated and deprotonated forms of  $^3DMB^*$  (HT and T, respectively) with the neutral and deprotonated forms of PTA (HPTA and PTA $^-$ , respectively):

$$k'_{PTA} = \alpha * \alpha_{HT}\alpha_{HPTA} + b * \alpha_{T}\alpha_{HPTA} + c * \alpha_{HT}\alpha_{PTA} + d * \alpha_{T}\alpha_{PTA}$$
 (6)

where  $\alpha$  is the mole fraction of each acid/base form of <sup>3</sup>DMB\* or PTA, and a, b, c, and d represent the reactivity of each combination of <sup>3</sup>DMB\* and PTA acid-base forms. To fit our data to this equation, initially we applied all parameters in the fitting. However, we found that b and c are not independent, while the value of d should be very low since  $k'_{PTA}$  values are essentially zero at higher pH. Thus in our second iteration we set parameters b and d to zero, but this resulted in a negative value of a, which is unreasonable (Figure. S6). We then set a, b, and d to zero, resulting in an equation that fits the data reasonably well (Figure 2), and gives a c value of 0.046 min<sup>-1</sup>. This shows that <sup>3</sup>DMB\* reacts more quickly with the deprotonated form of PTA, which is expected since this form is more electron rich than the neutral form. Also the sulfur radical of the PTA anion has a shorter lifetime, <sup>63</sup> leading to faster decarboxylation, compared to the equivalent radical of neutral PTA. Both forms of PTA seem to exhibit poor reactivity towards neutral <sup>3</sup>DMB\*. Overall, the strong pH dependence of the PTA-<sup>3</sup>DMB\* reaction, and the associated very low reactivity at high and low pH, is a weakness, but the probe works reasonably well under mildly acidic conditions, which are common for aerosol liquid water at our location in winter. 42 We also examined the pH dependence of PTA reacting with 3BP\* (Figure S7); here the rate constant increases with increasing pH, plateauing around pH 4, which also suggests that the deprotonated form of PTA is more reactive. To investigate PTA reactivity with OH, and its sensitivity to triplets with different energies, we determined the bimolecular rate constants of PTA with OH and two other triplets, 3'methoxyacetophenone (3MAP) and 2-acetonaphthone (2AN) at pH 4.2. The rate constants are shown in Table S2, while the triplet energies and reduction potentials are in Table S3. The rate constant of PTA with  ${}^33MAP^*$  is 3.1 ( $\pm$  0.4)  $\times$  10 ${}^9$  M ${}^{-1}$  s ${}^{-1}$ , which is statistically the same as with  ${}^3DMB^*$  (Table 1). However, the rate constant with <sup>3</sup>2AN\*, a weakly oxidizing triplet, is around 100 times lower, at 2.4 (±  $0.2) \times 10^7 \,\mathrm{M}^{-1} \,\mathrm{s}^{-1}$ . In contrast, for SYR at pH 5 the rate constant with  $^32\mathrm{AN}^*$  is only 2 times lower than the value with <sup>3</sup>DMB\* (Figure S8). <sup>14</sup> This apparent low reactivity of PTA with weakly oxidizing triplets

complicates determining triplet concentrations in environmental samples, where the relative amounts of

266

267

268

269

270

271

272

273

274

275

276

277

278

279

280

281

282

283

284

285

286

287

288

289

different energy triplets is unknown. However, measuring triplets with both PTA and SYR might allow determination of both highly and weakly oxidizing triplets. Because hydrogen peroxide ( $H_2O_2$ ) is formed during illumination of atmospheric waters<sup>73</sup>, we also investigated the potential dark reaction between PTA and  $H_2O_2$ . As shown in Figure S9, this reaction is negligible, with less than 2% of PTA loss after 2.5 hr of dark reaction with 100  $\mu$ M  $H_2O_2$ .

296

297

298

299

300

301

302

303

304

305

306

307

308

309

310

311

312

313

314

291

292

293

294

295

#### Dependence of IF<sub>PTA</sub> on SYR+Cu concentrations and EDC

Increasing DOM concentrations increases the inhibition of <sup>3</sup>C\*-induced oxidation, which decreases the rate of probe degradation.<sup>25</sup> To investigate the effect of DOM concentration on PTA decay by <sup>3</sup>C\*, we measured the inhibition factors of PTA and FFA as a function of SYR+Cu concentrations (at a fixed molar ratio of 70:1) with DMB as the triplet precursor. We also investigated the relationship between IF and electron donating capacity (EDC), which is correlated with the antioxidant capacity, phenolic content, and inhibition efficiency of DOM. 74-77 Moreover, Leresche et al. found that rate constants of quenching an aromatic amine radical cation by phenol and DOM increase with EDC.<sup>28</sup> We determined EDC using a method modified from Walpen et al. 78 and Yuan et al. 79, as described in SI Section S6. Our goal was to develop a relationship between IF and EDC so that we could predict  $IF_{PTA}$  in solutions using EDC, which is much simpler to measure than the corrected inhibition factor. Figure 3 shows inhibition factors for PTA and FFA, and IF<sub>PTA,corr</sub>, as a function of SYR concentration in solutions with triplet DMB: all three of these inhibition factors decrease with increasing SYR and Cu(II). With 420  $\mu$ M SYR and 6  $\mu$ M Cu(II),  $IF_{FFA}$  is 0.44 ( $\pm$  0.03), indicating that more than half of <sup>3</sup>DMB\* is quenched. At this concentration,  $IF_{PTA}$  is 0.23 ( $\pm$  0.01), showing high inhibition, corresponding to a  $IF_{PTA,corr}$  of 0.53 (± 0.04). We employed a kinetic model from Wenk et al. to fit the  $IF_{PTA,corr}$  data (SI Section S4).<sup>25</sup> In this model, the intermediate from probe oxidation can either undergo further irreversible oxidation to form products (with a first-order rate constant  $k_{ox}$ ), or be reduced by DOM to regenerate the

parent probe (with second-order rate constant  $k_{\text{red,DOM}}$ ). In this model the inverse of  $IF_{\text{PTA,corr}}$  can be expressed by:

$$\frac{1}{IF_{PTA\,corr}} = 1 + \frac{k_{red,DOM}}{k_{ox}}[SYR] \tag{7}$$

318

319

320

321

322

323

324

325

326

327

328

329

330

331

332

333

334

335

336

337

338

Figure 3B shows this fitting for our corrected PTA data. The linear regression has a slope of 0.0021 μM<sup>-1</sup>, while the inverse of this is  $[SYR]_{1/2}$ , i.e., the SYR concentration that causes  $IF_{PTA,corr}$  to equal 0.5. This concentration is 480 µM, a fairly high value that shows the resistance of PTA to inhibition. In Figure 3A we also show the regression fit to the  $IF_{FFA}$  data with Equation S10, which has the same functional form as Equation 7 but different physical meanings for the fitting parameters (Section S4). Based on the  $IF_{FFA}$ data, it takes approximately 300 µM SYR to quench half of the DMB triplets. Figure S11 shows the dependence of IF<sub>PTA</sub> and IF<sub>FFA</sub> on SYR using benzophenone as the triplet precursor. Compared with the DMB results, IF for both FFA and PTA are lower with <sup>3</sup>BP\*, likely because <sup>3</sup>BP\* is a more reactive triplet that is more rapidly quenched by SYR. However, IF<sub>PTA,corr</sub> with <sup>3</sup>BP\* does not behave in the same way as it does with <sup>3</sup>DMB\*, with the former showing an odd minimum at 70 μM SYR and a value approaching unity at higher SYR and Cu(II) concentrations. To investigate the relationship between inhibition and EDC, we fit a linear regression to the measured IF<sub>FFA</sub> and IF<sub>PTA,corr</sub> as a function of EDC in SYR+Cu solutions, particle water extracts, and SRFA at pH 4.2 (Figure 4). The y-intercept is set to 1, because at zero EDC there should be no inhibition (i.e., IF = 1). We have expressed the x-axis as the product of EDC (mmol  $e^-g_C^{-1}$ ) and DOC (g C L<sup>-1</sup>) with units of mmol e L-1 so that we can quantify the total amount of electrons that DOM can donate in a solution. As shown in Figure 4, IF<sub>FFA</sub> values decrease with increasing EDC×DOC, consistent with the idea that higher DOC corresponds to more triplet quenching. The SRFA result is an outlier, with an  $IF_{FFA}$  value close to 2, suggesting that the interaction of DOM and <sup>3</sup>DMB\* forms species that react with FFA, accelerating its decay. Other than that,  $IF_{FFA}$  correlates modestly well with EDC ( $R^2 = 0.59$ ). Since values of  $IF_{FFA}$ greater than 1 indicate no suppression of triplet concentrations, under this condition, we assume that

 $\underline{IF}_{P,corr}$  equals  $IF_P$  (Section S4) for all solutions. As shown in Figure 4B,  $IF_{PTA,corr}$  shows a good correlation with EDC in the SYR+Cu solutions, but the relationship is poor for the SRFA and PME solutions, suggesting EDC is a poor predictor for probe inhibition across different samples. This poor relationship in the natural samples might be because of a contribution to EDC from Fe(II)<sup>80</sup>, which we did not measure in our samples.

For our last experiments, we used PTA and SYR to evaluate probe inhibition and determine triplet

344

345

346

347

348

349

350

351

352

353

354

355

356

357

358

359

360

361

362

339

340

341

342

343

#### Determination of [3C\*] in PME using PTA as the triplet probe

concentrations in four aqueous extracts of fine particles. These PMEs were prepared from PM<sub>2.5</sub> samples collected in Davis, CA; extract DOC concentrations range from 9.9 to 105 mg C L<sup>-1</sup>. Sample details are provided in Table S4: PME1 is from a sample collected on a clear summer day; PME2 and PME3 are extracted from winter samples with residential wood burning; and PME4 represents air that was heavily impacted by summer wildfires. As shown in Figure 5A, IF<sub>FFA</sub> in the PMEs is 1 or greater, indicating that <sup>3</sup>DMB\* is not significantly quenched by DOM. In contrast, based on the rate constants of aquatic DOM quenching <sup>3</sup>C\* determined by Wenk et al.,<sup>59</sup> we would expect DOM to quench 13 – 30% of triplets at our highest DOC concentration of 105 mg C L<sup>-1</sup>. Though IF<sub>FFA</sub> indicates little or no quenching of triplets by DOM in PME samples, we continue to use  $IF_{P,corr}$  for the rest of this discussion; as described in Section S4, when  $IF_{FFA} > 1$ , we do not make a correction to the probe inhibition factor and assume  $IF_{P,corr} = IF_P$ . In PME1 with low DOC (9.9 mg  $C L^{-1}$ ),  $IF_{SYR,corr}$  and  $IF_{PTA,corr}$  are both around 0.76, indicating neither is heavily impacted by DOM in this relatively dilute PME. For PME2 and PME3, which have moderate DOC (64 and 69 mg C L<sup>-1</sup>), corrected IF values for SYR are 0.50 ( $\pm$  0.11) and 0.16 ( $\pm$  0.03), respectively, and for PTA are 1.2 ( $\pm$  0.1) and 1.3 ( $\pm$ 0.1). Thus, while SYR decay by <sup>3</sup>DMB\* is significantly inhibited by DOM, PTA is not. For PME4, the extract from the wildfire particles, corrected IF values for SYR and PTA are 0.31 ( $\pm$  0.02) and 0.60 ( $\pm$ 

0.04), respectively. Thus both probes are inhibited in this sample (though PTA is less affected), possibly because of abundant antioxidant phenols, which are present in biomass-burning aerosols. This is consistent with the high EDC value of PME4 (Table S4). However, there is no consistent trend of *IF* values with DOC, though we expected that the extent of inhibition would increase with DOC.

We next determined triplet concentrations in the four PM extracts based on SYR and PTA data. We also measured OH and O2\* concentrations so that we could subtract their contributions to SYR and PTA decay in PME (Table S5). OH accounts for 5% – 17% of SYR decay and 7% – 28% of PTA decay, while O2\* contributes 9% – 17% and 4% – 9%, respectively. Based on our past work, we assume that The PME have similar reactivity as DMB\* and use the second-order rate constants of each probe with DMB\* to calculate the C\*\* concentration from each set of probe data. We then correct each triplet

concentration for inhibition using<sup>33,83</sup>

$$[{}^{3}C^{*}]_{P,corr} = \frac{[{}^{3}C^{*}]_{P}}{IF_{P,corr}}$$
(8)

As described in Section S4, when  $IF_{P,corr}$  is greater than 1 (which indicates no inhibition) we do not make a correction for the  ${}^{3}C^{*}$  concentration, i.e., we use  $[{}^{3}C^{*}]_{P,corr} = [{}^{3}C^{*}]_{P}$ . As Figure 5B shows, uncorrected  ${}^{3}C^{*}$  concentrations derived from PTA range from  $(0.02-2) \times 10^{-13}$  M,

while SYR-derived [ ${}^{3}$ C\*] are in the range of  $(0.07 - 2) \times 10^{-13}$  M, with [ ${}^{3}$ C\*]<sub>PTA</sub>/[ ${}^{3}$ C\*]<sub>SYR</sub> ratios of 0.3 to 2.2. Based on the properties of these two probes (Table 1), we expected that uncorrected triplet concentrations would be higher with PTA as a probe (since it is less susceptible to inhibition than SYR), but this expectation is only true for PME2 and PME3. With *IF* correction, [ ${}^{3}$ C\*]<sub>P,corr</sub> increases by factors of 1 - 1.7 for PTA and 1.3 - 4.8 for SYR, respectively, compared to the corresponding uncorrected value. We also expected that correcting for inhibition would yield similar [ ${}^{3}$ C\*] for the two probes. However, we only observe this in PME2, while for the other three samples the triplet concentration from *IF*-corrected

PTA data is lower than the concentration from *IF*-corrected SYR data. The range of

 $[^{3}C^{*}]_{PTA,corr}/[^{3}C^{*}]_{SYR,corr}$  is 0.27-0.88 with a mean value of 0.45. A ratio less than 1 might be explained

by the higher oxidation potential of PTA (1.47 V vs. SHE, estimated using the Marcus equation) than SYR (~1.17 V vs. SHE), 62,84 suggesting that PTA can miss weakly oxidizing triplets that are captured by SYR. This is consistent with the PTA having a much lower rate constant than SYR with the weakly oxidizing 2-acetonapthone triplet (Figure S8 and Table S3). PME4, the wildfire sample, has the lowest value of [<sup>3</sup>C\*]<sub>PTA.corr</sub>/[<sup>3</sup>C\*]<sub>SYR.corr</sub>, suggesting that <sup>3</sup>C\* in PME4 are less oxidizing than those in other samples. This is consistent with the observation that highly aromatic DOM, such as in wildfire particles.<sup>85</sup> might show a lower triplet reactivity.<sup>25</sup> These observations indicate that it would be useful to consider oxidation potential as another important factor in future work on triplet probe selection, since this influences the pool of oxidizing triplets that can be quantified. Our results in the particle extracts show that PTA is less sensitive to inhibition to DOM than SYR, as expected from our lab solutions, but we also found some disadvantages to PTA. For one, the <sup>3</sup>C\* concentration obtained by PTA is lower than that from SYR after IF correction, suggesting PTA is "missing" the weakly oxidizing triplets that are seen with SYR. In addition, the PTA reactivity with triplets depends on pH, which reduces its utility. As for SYR, it suffers more from inhibition but captures more of the total pool of oxidizing <sup>3</sup>C\*; the same is probably true for other phenols such as TMP. Given the different sensitivities of PTA and SYR to weakly oxidizing triplets, applying both triplet probes might provide a more comprehensive understanding of <sup>3</sup>C\* concentrations as well as their oxidizing character. Finally, we can combine the singlet molecular oxygen and oxidizing triplet results from our PM extracts to gain more information about SYR and PTA as triplet probes. As described by McNeill and Canonica<sup>1</sup>, under dilute conditions the ratio [\(^1O\_2\*\)]/[\(^3CDOM\*\)], where \(^3CDOM\*\) denotes the total triplet pool, is proportional to the product  $f_{\Delta} \times k_{O2}$ , where  $f_{\Delta}$  is the fraction of <sup>3</sup>CDOM\*-O<sub>2</sub> interactions that form singlet oxygen and  $k_{02}$  is the second-order rate constant for this interaction. Based on surface water values for these parameters  $^{86,87}$ ,  $\lceil ^{1}O_{2}* \rceil / \lceil ^{3}CDOM* \rceil \approx 0.3$ , while the average ( $\pm 1 \sigma$ ) ratio of  $\lceil ^{1}O_{2}* \rceil / \lceil ^{3}C* \rceil_{SYR}$  in our PM extracts is  $7.9 \pm 3.4$  (Table S5). This 26-fold higher ratio in PME is probably caused by a combination of three factors. First, we are only measuring oxidizing triplets (<sup>3</sup>C\*), a subset of the total

387

388

389

390

391

392

393

394

395

396

397

398

399

400

401

402

403

404

405

406

407

408

409

410

triplet pool, so  $[{}^{1}O_{2}*]/[{}^{3}C*]$  will be equal to or larger than  $[{}^{1}O_{2}*]/[{}^{3}CDOM*]$ . Second, the  ${}^{3}DMB*$  rate constants with SYR and PTA that we use to determine  $[{}^{3}C*]$  might be larger than the rate constants of natural triplets with our probes, which would cause us to underestimate concentrations of oxidizing triplets. Third, if triplets in atmospheric particles have higher values of  $f_{\Delta}$  and  $k_{O2}$  than triplets in surface waters, this would increase the  $[{}^{1}O_{2}*]/[{}^{3}CDOM*]$  ratio; for example, using values from model triplets yields a ratio of  $1.8^{14}$ . While the first factor – that oxidizing triplets are only a fraction of the total triplet pool – certainly accounts for some of the difference between measured and calculated oxidant ratios, the contributions of the second and third factors are currently unclear.

#### **Present Addresses**

†Now at Department of Chemistry, University of Washington, Seattle, WA 98195, United States.

#### **Supporting Information**

Additional method information including chemicals, illumination and kinetic analysis, particle collection and extraction, determination of OH and  $^{1}O_{2}*$  concentration, and EDC determination; derivation of equations; additional figures of dependence of inhibition factor on DOM concentration; dependence of PTA absorbance and decay rate on pH; dark reaction of PTA with  $H_{2}O_{2}$ ; tabulated rate constants of PTA with oxidants; summary of particle water extract information. This information is available free of charge via the Internet at http://pubs.acs.org.

#### ACKNOWLEDGEMENTS

This work was funded by the National Science Foundation grant (AGS-1649212 and AGS-2220307), the
California Agricultural Experiment Station (CA-D-LAW-6403-RR) and a Jastro-Shields Research Award
and Donald G. Crosby Fellowship to L.M. We thank Keith J. Bein for the loan of, and assistance with, a
PM <sub>2.5</sub> high-volume sampler and Wenqing Jiang, Christopher Niedek, and Qi Zhang for DOC and ions
analysis. We also thank the anonymous reviewers for their helpful and constructive comments.

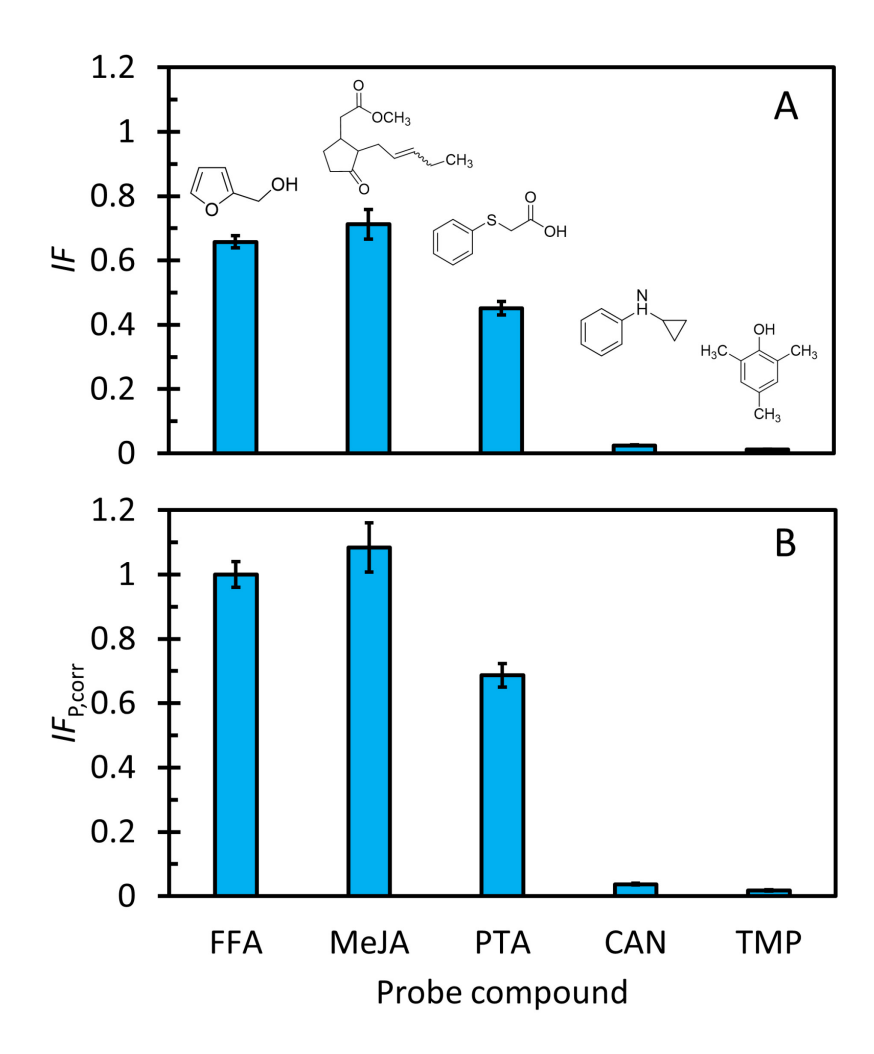


**Figure 1.** Inhibition factor (Panel A) and the corrected inhibition factors (Panel B; equation 5) for triplet probes reacting with  ${}^{3}BP^{*}$  in solutions containing 70  $\mu$ M SYR and 1  $\mu$ M Cu(II) at pH 4.2. Error bars represent  $\pm 1$  standard error propagated from linear regressions.

439

440

441 442

443

444

445

446

447

448

449

450

					% (k' <sub>3C*</sub> ) in			
Class	Compound	$k_{\text{P+3DMB*}}  (\text{M}^{-1}  \text{s}^{-1})$	$k_{\rm P+1O2*}  ({ m M}^{-1}  { m s}^{-1})$	$k_{\rm P+3DMB*}/k_{\rm P+1O2*}$	$PME^{b}$	$IF^{c}$	$IF_{P,\mathrm{corr}}^{\mathrm{d}}$	$j (s^{-1})^e$
Sulfide	(Phenylthio)acetic acid (PTA)	$2.5 \ (\pm 0.6) \times 10^{9f}$	$8.8 \ (\pm 0.6) \times 10^6$	284 (±71)	90	0.45 (±0.02)	0.69 (±0.04)	$1.0 (\pm 0.1) \times 10^{-5}$
	Methyl jasmonate (MeJA)	$4.1~(\pm 1.0) \times 10^8$	$6.0~(\pm 0.7) \times 10^6$	68 (±18)	67	0.71 (±0.05)	1.08 (±0.08)	n/a <sup>g</sup>
	Terpineol (TPN)	$2.1 \ (\pm 0.2) \times 10^8$	$1.7 (\pm 0.1) \times 10^6$	121 (±16)	64	$0.65~(\pm 0.01)$	$0.99~(\pm 0.03)$	n/a
Alkene	Pulegone	$4.7 (\pm 1.2) \times 10^9$	$3.7 (\pm 0.4) \times 10^7$	128 (±37)	85	$0.25~(\pm 0.02)$	$0.30~(\pm 0.03)$	$1.4 (\pm 0.3) \times 10^{-6}$
	cis-3-Hexenyl acetate	$2.7 (\pm 0.7) \times 10^8$	$6.2 (\pm 1.4) \times 10^6$	44 (±15)	57	$ND^{h}$	ND	n/a
	Prenyl acetate	$1.5 (\pm 0.4) \times 10^8$	$1.0 \ (\pm 0.2) \times 10^7$	15 (±5)	34	$0.61~(\pm 0.06)$	$0.93~(\pm 0.09)$	n/a
	Linalool	$1.7 (\pm 0.4) \times 10^9$	$1.5 (\pm 0.2) \times 10^8$	11 (±3)	35	ND	ND	n/a
Amine	Atenolol (ANL)	$1.0~(\pm 0.3) \times 10^8$	$1.8~(\pm 0.2) \times 10^6$	55 (±16)	46	$0.56~(\pm 0.03)$	$0.86~(\pm 0.05)$	n/a
	<i>N</i> -cyclopropylaniline (CAN)	n/a <sup>i</sup>	$2.8 \ (\pm 0.6) \times 10^9$	n/a	n/a	0.03 (±0.01)	0.04 (±0.01)	$5.2 (\pm 0.8) \times 10^{-4}$
Anilines	3,5-dichloro- <i>N</i> -cyclopropylaniline (DCCAN)	$1.5~(\pm 0.2) \times 10^{10}$	$6.0~(\pm 1.1) \times 10^8$	24 (±5)	54	0.09 (±0.01)	0.14 (±0.01)	$2.4 \ (\pm 0.1) \times 10^{-4}$
	Syringol (SYR)	$3.9 \ (\pm 0.7) \times 10^{9j}$	$3.6 \ (\pm 0.7) \times 10^{7k}$	107 (±29)	82	n/a	n/a	<3.6 ×10 <sup>-61</sup>
Phenols	2,4,6-trimethylphenol (TMP)	$2.4 (\pm 0.4) \times 10^9$	$6.2~(\pm 1.0) \times 10^{7k}$	39 (±9)	64	0.01 (±0.01)	0.02 (±0.01)	n/a

<sup>&</sup>lt;sup>a</sup> Values were determined at 20 °C. Errors in parentheses are 1 standard error.

<sup>&</sup>lt;sup>b</sup>Percentage of probe decay due to triplet reaction in a concentrated particle extract, calculated at an extract particle mass/water mass ratio of  $4 \times 10^{-3}$  μg PM/μg H<sub>2</sub>O based on results from Kaur et al., <sup>16</sup> where <sup>•</sup>OH, <sup>3</sup>C\*, and <sup>1</sup>O<sub>2</sub>\* concentrations were  $1.7 \times 10^{-15}$ ,  $4.1 \times 10^{-13}$ , and  $8.5 \times 10^{-12}$  M, respectively.

 $<sup>^{</sup>c}$  Inhibition factor in solutions containing 70  $\mu M$  SYR and 1  $\mu M$  Cu. We used 15  $\mu M$  BP as the triplet precursor, except for pulegone, where we used 80  $\mu M$  DMB.

 $<sup>^{\</sup>rm d}IF_{\rm corrected}$  is calculated with equation 5 and  $IF_{\rm FFA}$  values., which are 0.66 with 15  $\mu$ M BP and 0.83 with 80  $\mu$ M DMB.

eThe direct photolysis rate constants are determined at pH 4.2 and normalized to sunlight conditions at midday on the winter solstice at Davis (solar zenith =  $62^{\circ}$ ;  $j_{2NB,win} = 0.0070 \text{ s}^{-1}$ ).

<sup>&</sup>lt;sup>f</sup>The rate constant is determined with the direct measurement method, see details in Figure S8.

<sup>&</sup>lt;sup>g</sup>Not applicable.

<sup>&</sup>lt;sup>h</sup>Not determined.

<sup>&</sup>lt;sup>i</sup>The rate constant of CAN measured with the relative rate method (>10<sup>11</sup> M<sup>-1</sup> s<sup>-1</sup>) is much higher than the diffusion-controlled rate constant (approximately 10<sup>10</sup> M<sup>-1</sup> s<sup>-1</sup>), indicating a problem. One possibility is that an oxidant other than triplet DMB is responsible for most of the probe loss.

<sup>451 &</sup>lt;sup>j</sup>From Smith et al. <sup>58</sup>

<sup>452 &</sup>lt;sup>k</sup>From Tratnyek et al.<sup>88</sup>

From Kaur et al. 14

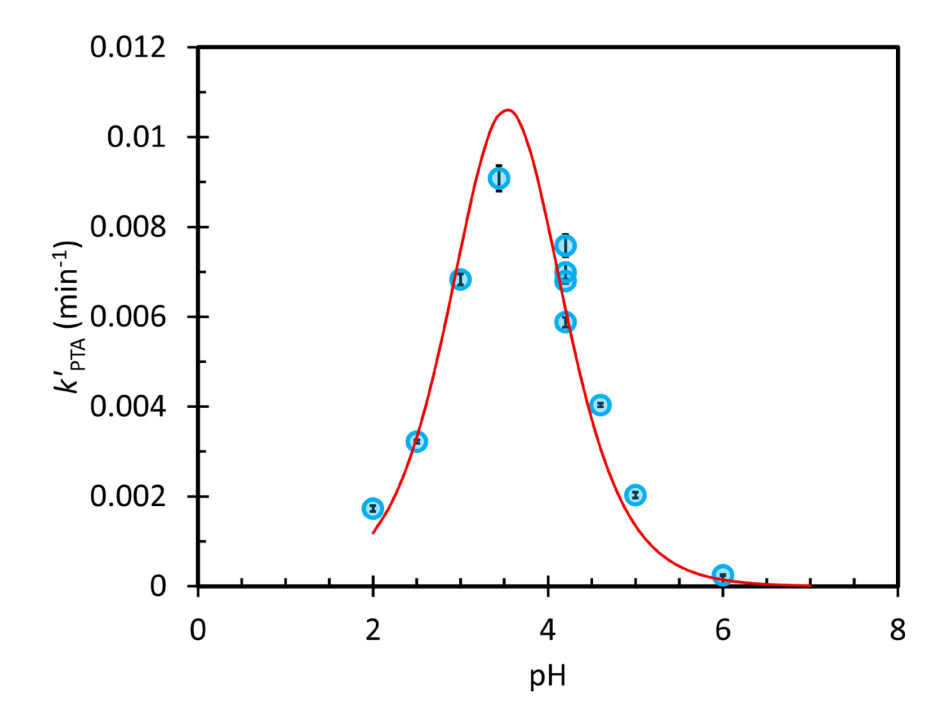


**Figure 2.** Influence of pH on the first-order PTA decay rate constant due to the DMB triplet; rate constants are corrected for direct photodegradation and are normalized to a  $j_{2NB}$  value of 0.007 s<sup>-1</sup>. Solutions contained 10 μM DMB, 10 μM PTA, and either H<sub>2</sub>SO<sub>4</sub> or NaOH for pH adjustment and were maintained at 20 °C. The red line is the regression fit to eq 6, with p $K_a$  values of <sup>3</sup>DMB\* and PTA of 3.5 and 3.56, respectively, <sup>72</sup> and values of a, b, and d set as zero. The resulting fitted value of c is 0.046 min<sup>-1</sup>. Error bars represent ±1 SE, propagated from the linear regressions and  $j_{2NB}$ .

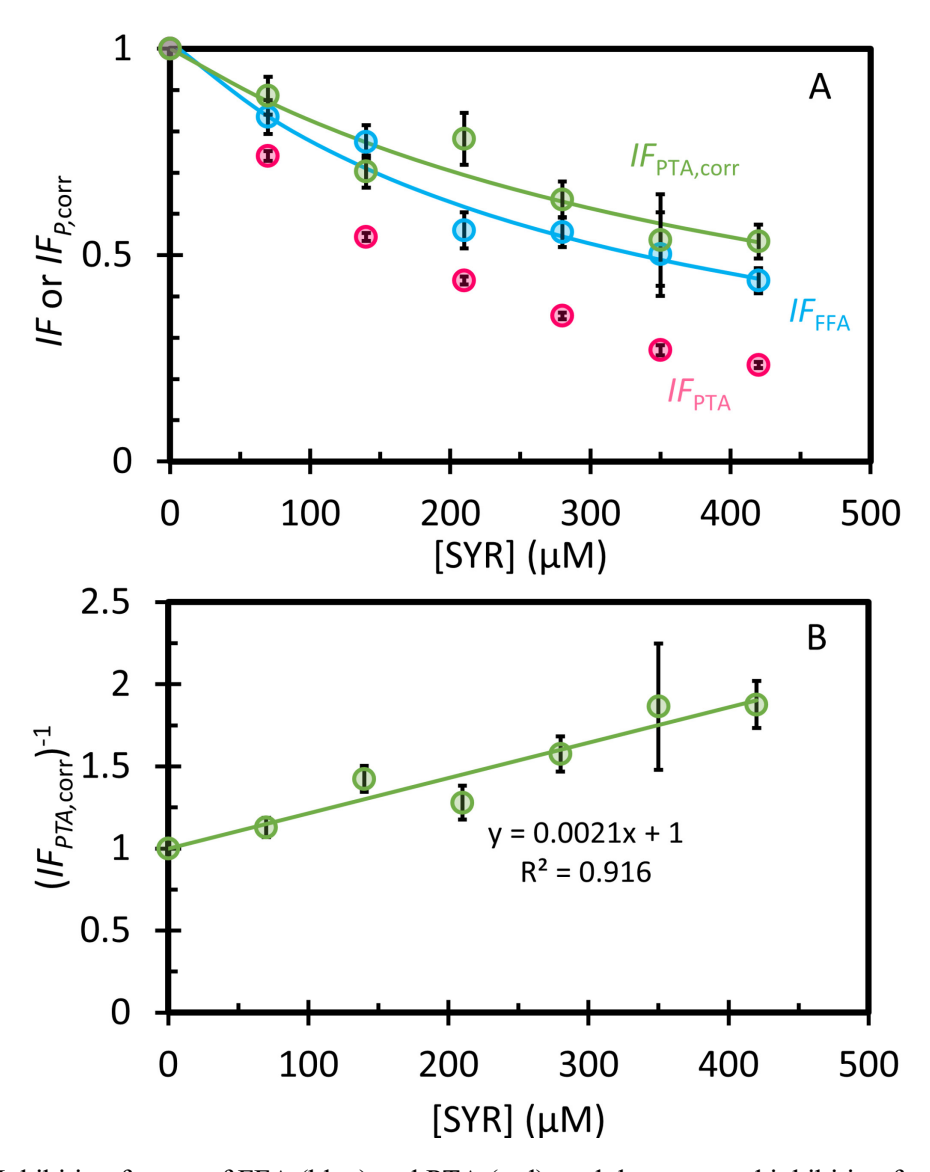


**Figure 3.** (A) Inhibition factors of FFA (blue) and PTA (red), and the corrected inhibition factor of PTA (green) as a function of SYR concentration with 80 μM DMB as the triplet precursor in solution at pH 4.2; solutions also contain Cu(II) at a molar ratio of SYR/Cu(II) of 70:1. The solid lines represent linear regression fits between the inverse of IF values versus the SYR concentration. (B) The inverse of *IF* corrected,PTA (from Panel A) as a function of SYR concentration. For both panels, error bars represent ±1 SE, propagated from the linear regressions.

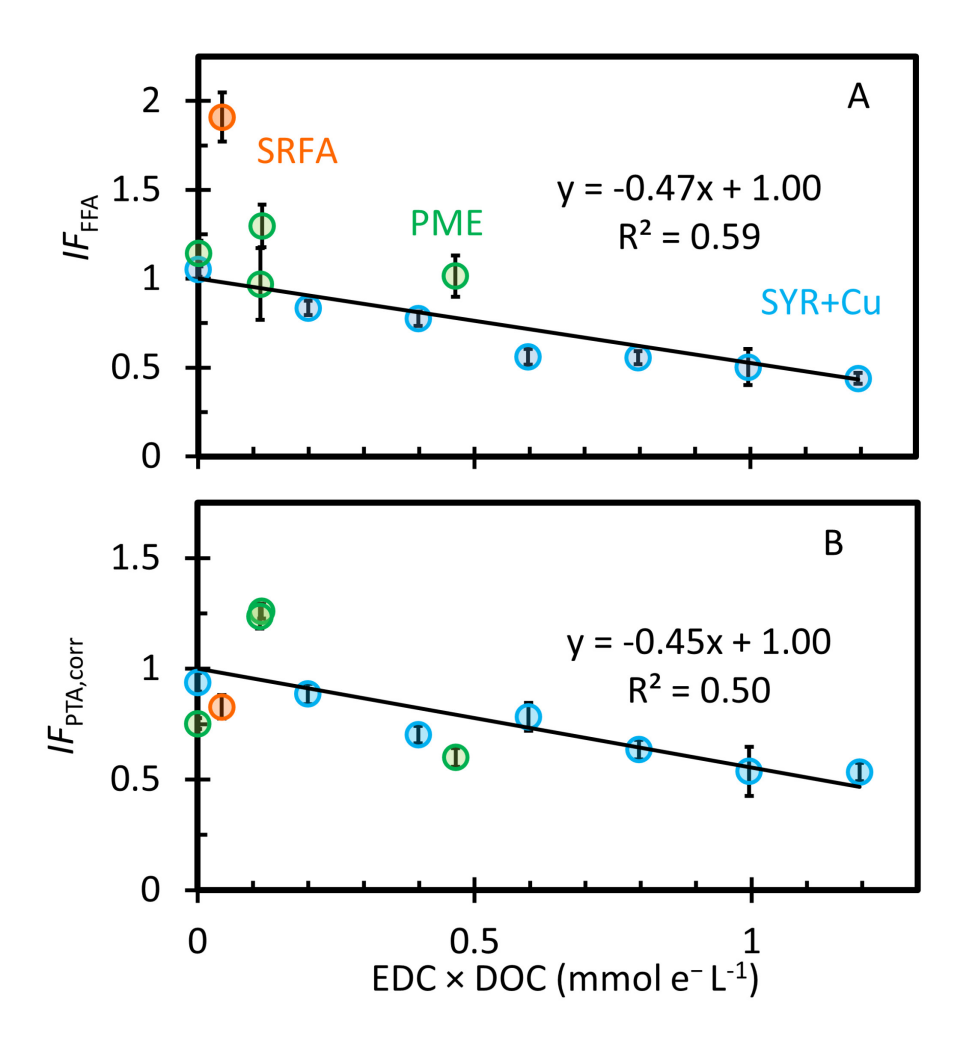


**Figure 4.** The inhibition factor of FFA (Panel A) and corrected inhibition factor of PTA (Panel B) as a function of the product of electron donating capacity (EDC) with dissolved organic carbon (DOC) in SRFA (orange), PME (green), and SYR+Cu (blue) solutions with 80  $\mu$ M DMB as the triplet precursor at pH 4.2. Error bars represent  $\pm 1$  SE, propagated from the linear regressions of the FFA and/or PTA decay plots. Data are available in Table S3. Lines represent the linear regressions of all data points.

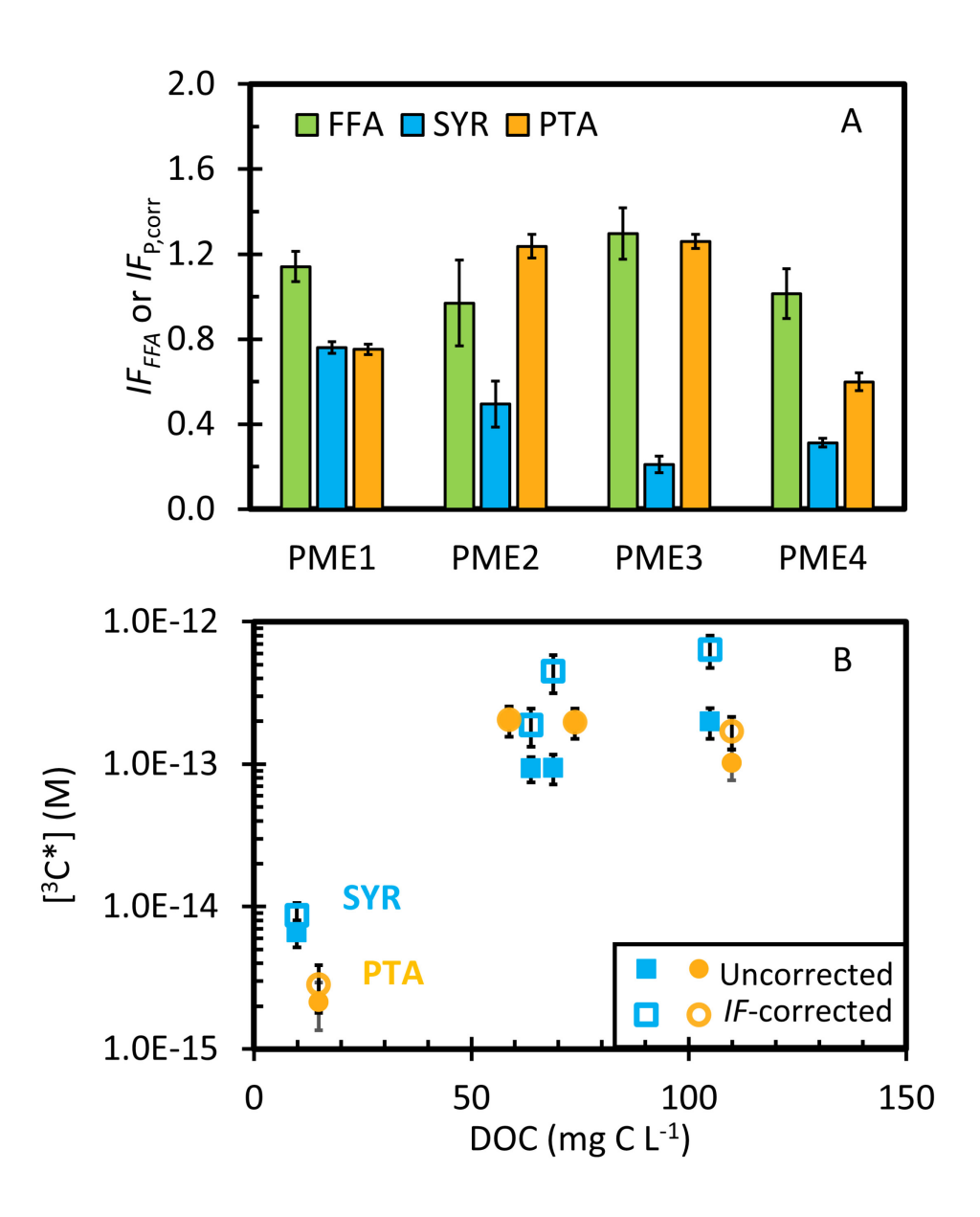


**Figure 5.** (A) Inhibition factors of FFA and corrected inhibition factors of SYR and PTA in particle extracts with 80 μM DMB as the triplet precursor at pH 4.2. (B) Raw (solid symbols) and inhibition-corrected (open symbols) concentrations of <sup>3</sup>C\* determined from SYR (blue squares) and PTA (yellow circles) as a function of dissolved organic carbon concentration. To separate the SYR and PTA results, we add 5 mg C L<sup>-1</sup> to the DOC concentration for each PTA-derived value. To more clearly show the PME2 and PME3 results, we subtract 5 mg C L<sup>-1</sup> from the former when plotting it. The uncorrected and *IF*-corrected <sup>3</sup>C\* derived by PTA values are overlapping for PME2 and PME3. Error bars represent ±1 SE, propagated from the regressions of probe decay and second-order rate constants.

#### 491 **REFERENCES**

- 492 (1) McNeill, K.; Canonica, S. Triplet state dissolved organic matter in aquatic 493 photochemistry: reaction mechanisms, substrate scope, and photophysical properties. 494 *Environ. Sci. Process. Impacts* **2016**, *18*, 1381–1399.
- 495 (2) Remucal, C. K. The role of indirect photochemical degradation in the environmental fate of pesticides: a review. *Environ. Sci. Process. Impacts* **2014**, *16*, 628–653.
- 497 (3) Challis, J. K.; Hanson, M. L.; Friesen, K. J.; Wong, C. S. A critical assessment of the 498 photodegradation of pharmaceuticals in aquatic environments: defining our current 499 understanding and identifying knowledge gaps. *Environ. Sci. Process. Impacts* **2014**, *16*, 500 672–696.
- 501 (4) Aregahegn, K. Z.; Nozière, B.; George, C. Organic aerosol formation photo-enhanced by 502 the formation of secondary photosensitizers in aerosols. *Faraday Discuss* **2013**, *165*, 123– 503 134.
- 504 (5) González Palacios, L.; Corral Arroyo, P.; Aregahegn, K. Z.; Steimer, S. S.; Bartels-505 Rausch, T.; Nozière, B.; George, C.; Ammann, M.; Volkamer, R. Heterogeneous 506 photochemistry of imidazole-2-carboxaldehyde: HO<sub>2</sub> radical formation and aerosol 507 growth. *Atmos. Chem. Phys.* **2016**, *16*, 11823–11836.
- 508 (6) Rossignol, S.; Aregahegn, K. Z.; Tinel, L.; Fine, L.; Nozière, B.; George, C. Glyoxal induced atmospheric photosensitized chemistry leading to organic aerosol growth.

  510 Environ. Sci. Technol. 2014, 48, 3218–3227.
- Wang, X.; Gemayel, R.; Hayeck, N.; Perrier, S.; Charbonnel, N.; Xu, C.; Chen, H.; Zhu, C.; Zhang, L.; Wang, L.; Nizkorodov, S.A.; Wang, X; Wang, Z.; Wang T.; Mellouki, A.; Riva, M.; Chen, J.; George, C. Atmospheric photosensitization: A new pathway for sulfate formation. *Environ. Sci. Technol.* **2020**, *54*, 3114–3120.
- Ossola, R.; Clerc, B.; McNeill, K. Mechanistic insights into dissolved organic sulfur photomineralization through the study of cysteine sulfinic acid. *Environ. Sci. Technol.* **2020**, *54*, 13066–13076.
- Ossola, R.; Tolu, J.; Clerc, B.; Erickson, P. R.; Winkel, L. H. E.; McNeill, K.
   Photochemical Production of Sulfate and Methanesulfonic Acid from Dissolved Organic
   Sulfur. Environ. Sci. Technol. 2019, 53, 13191–13200.
- 521 (10) Anastasio, C.; Faust, B. C.; Rao, C. J. Aromatic carbonyl compounds as aqueous-phase 522 photochemical sources of hydrogen peroxide in acidic sulfate aerosols, fogs, and clouds. 523 1. Non-phenolic methoxybenzaldehydes and methoxyacetophenones with reductants 524 (phenols). *Environ. Sci. Technol.* **1996**, *31*, 218–232.

- 525 (11) Corral Arroyo, P.; Bartels-Rausch, T.; Alpert, P. A.; Dumas, S.; Perrier, S.; George, C.;
- Ammann, M. Particle-Phase Photosensitized Radical Production and Aerosol Aging.
- 527 Environ. Sci. Technol. **2018**, 52, 7680–7688.
- 528 (12) Zepp, R. G.; Wolfe, N. L.; Baughman, G. L.; Hollis, R. C. Singlet oxygen in natural waters. *Nature* **1977**, *267*, 421.
- 530 (13) Zepp, R. G.; Schlotzhauer, P. F.; Sink, R. M. Photosensitized transformations involving
- electronic energy transfer in natural waters: role of humic substances. *Environ. Sci.*
- 532 *Technol.* **1985**, *19*, 74–81.
- Kaur, R.; Anastasio, C. First measurements of organic triplet excited states in atmospheric waters. *Environ. Sci. Technol.* **2018**, *52*, 5218–5226.
- Kaur, R.; Anastasio, C. Light absorption and the photoformation of hydroxyl radical and singlet oxygen in fog waters. *Atmos. Environ.* **2017**, *164*, 387–397.
- 537 (16) Kaur, R.; Labins, J. R.; Helbock, S. S.; Jiang, W.; Bein, K. J.; Zhang, Q.; Anastasio, C.
- Photooxidants from brown carbon and other chromophores in illuminated particle
- extracts. Atmos. Chem. Phys. **2019**, 19, 6579–6594.
- 540 (17) Ma, L.; Guzman, C.; Niedek, C.; Tran, T.; Zhang, Q.; Anastasio, C. Kinetics and mass
- yields of aqueous secondary organic aerosol from highly substituted phenols reacting with
- 542 a triplet excited state. *Environ. Sci. Technol.* **2021**, *55*, 5772–5781.
- 543 (18) Schmitt, M.; Moor, K. J.; Erickson, P. R.; McNeill, K. Sorbic acid as a triplet probe:
- reactivity of oxidizing triplets in dissolved organic matter by direct observation of
- aromatic amine oxidation. *Environ. Sci. Technol.* **2019**, *53*, 8087–8096.
- 546 (19) Grebel, J. E.; Pignatello, J. J.; Mitch, W. A. Sorbic acid as a quantitative probe for the
- formation, scavenging and steady-state concentrations of the triplet-excited state of
- organic compounds. Water Res. **2011**, 45, 6535–6544.
- 549 (20) Zhou, H.; Yan, S.; Ma, J.; Lian, L.; Song, W. Development of Novel Chemical Probes for
- Examining Triplet Natural Organic Matter under Solar Illumination. *Environ. Sci.*
- 551 *Technol.* **2017**, *51*, 11066–11074.
- 552 (21) Moor, K. J.; Schmitt, M.; Erickson, P. R.; McNeill, K. Sorbic Acid as a Triplet Probe:
- Triplet Energy and Reactivity with Triplet-State Dissolved Organic Matter via 102
- Phosphorescence. *Environ. Sci. Technol.* **2019**, *53*, 8078–8086.
- 755 (22) Rosario-Ortiz, F. L.; Canonica, S. Probe compounds to assess the photochemical activity
- of dissolved organic matter. Environ. Sci. Technol. 2016, 50, 12532–12547.
- 557 (23) Maizel, A. C.; Remucal, C. K. The effect of probe choice and solution conditions on the
- apparent photoreactivity of dissolved organic matter. Environ. Sci. Process. Impacts
- **2017**, *19*, 1040–1050.

- Canonica, S.; Laubscher, H.-U. Inhibitory effect of dissolved organic matter on tripletinduced oxidation of aquatic contaminants. *Photochem. Photobiol. Sci.* **2008**, *7*, 547.
- Wenk, J.; von Gunten, U.; Canonica, S. Effect of dissolved organic matter on the transformation of contaminants induced by excited triplet states and the hydroxyl radical. *Environ. Sci. Technol.* **2011**, *45*, 1334–1340.
- Wenk, J.; Canonica, S. Phenolic antioxidants inhibit the triplet-induced transformation of anilines and sulfonamide antibiotics in aqueous solution. *Environ. Sci. Technol.* **2012**, *46*, 5455–5462.
- Leresche, F.; von Gunten, U.; Canonica, S. Probing the Photosensitizing and Inhibitory
   Effects of Dissolved Organic Matter by Using N,N-dimethyl-4-cyanoaniline (DMABN).
   Environ. Sci. Technol. 2016, 50, 10997–11007.
- 571 (28) Leresche, F.; Ludvíková, L.; Heger, D.; von Gunten, U.; Canonica, S. Quenching of an aniline radical cation by dissolved organic matter and phenols: A laser flash photolysis study. *Environ. Sci. Technol.* **2020**, *54*, 15057–15065.
- Weinberg, D. R.; Gagliardi, C. J.; Hull, J. F.; Murphy, C. F.; Kent, C. A.; Westlake, B. C.;
   Paul, A.; Ess, D. H.; McCafferty, D. G.; Meyer, T. J. Proton-Coupled Electron Transfer.
   Chem. Rev. 2012, 112, 4016–4093.
- 577 (30) Pan, Y.; Garg, S.; Waite, T. D.; Yang, X. Copper Inhibition of Triplet-Induced Reactions 578 Involving Natural Organic Matter. *Environ. Sci. Technol.* **2018**, *52*, 2742–2750.
- 579 (31) Pan, Y.; Ruan, X.; Garg, S.; Waite, T. D.; Lei, Y.; Yang, X. Copper Inhibition of Triplet-580 Sensitized Phototransformation of Phenolic and Amine Contaminants. *Environ. Sci.* 581 *Technol.* **2020**, *54*, 9980–9989.
- 582 (32) Remke, S. C.; Bürgin, T. H.; Ludvíková, L.; Heger, D.; Wenger, O. S.; von Gunten, U.; 583 Canonica, S. Photochemical oxidation of phenols and anilines mediated by phenoxyl 584 radicals in aqueous solution. *Water Res.* **2022**, 118095.
- McCabe, A. J.; Arnold, W. A. Reactivity of triplet excited states of dissolved natural organic matter in stormflow from mixed-use watersheds. *Environ. Sci. Technol.* **2017**, *51*, 9718–9728.
- 588 (34) Bodhipaksha, L. C.; Sharpless, C. M.; Chin, Y.-P.; Sander, M.; Langston, W. K.; 589 MacKay, A. A. Triplet photochemistry of effluent and natural organic matter in whole 590 water and isolates from effluent-receiving rivers. *Environ. Sci. Technol.* **2015**, *49*, 3453– 591 3463.
- 592 (35) Pflug, N. C.; Schmitt, M.; McNeill, K. Development of N-Cyclopropylanilines to Probe 593 the Oxidative Properties of Triplet-State Photosensitizers. *Environ. Sci. Technol.* **2019**, 594 53, 4813–4822.
- 595 (36) Leenheer, J. A.; Croué, J.-P. Peer reviewed: characterizing aquatic dissolved organic 596 matter. *Environ. Sci. Technol.* **2003**, *37*, 18A–26A.

- 597 (37) Ervens, B.; Turpin, B. J.; Weber, R. J. Secondary organic aerosol formation in cloud 598 droplets and aqueous particles (aqSOA): a review of laboratory, field and model studies. 599 Atmos. Chem. Phys. **2011**, 11, 11069–11102.
- 600 (38) McNeill, V. F. Aqueous organic chemistry in the atmosphere: sources and chemical processing of organic aerosols. *Environ. Sci. Technol.* **2015**, *49*, 1237–1244.
- 602 (39) Ervens, B. Progress and problems in modeling chemical processing in cloud droplets and 603 wet aerosol particles. In *Multiphase environmental chemistry in the atmosphere*; Hunt, S. 604 W.; Laskin, A.; Nizkorodov, S. A., Eds.; ACS Symposium Series; American Chemical 605 Society: Washington, DC, 2018; Vol. 1299, pp. 327–345.
- 606 (40) Battaglia Jr., M. A.; Weber, R. J.; Nenes, A.; Hennigan, C. J. Effects of water-soluble organic carbon on aerosol pH. *Atmos. Chem. Phys.* **2019**, *19*, 14607–14620.
- 608 (41) Pye, H. O. T.; Nenes, A.; Alexander, B.; Ault, A. P.; Barth, M. C.; Clegg, S. L.; Collett Go9 Jr., J. L.; Fahey, K. M.; Hennigan, C. J.; Herrmann, H.; Kanakidou, M.; Kelly, J.; Ku, I-T.; McNeill, V. F.; Riemer, N.; Schaefer, T.; Shi, G.; Tilgner, A.; Walker, J.T.; Wang, T.; Weber, R.; Xing, J.; Zaveri, R.A.; Zuend A. The acidity of atmospheric particles and clouds. Atmos. Chem. Phys. 2020, 20, 4809–4888.
- Parworth, C. L.; Young, D. E.; Kim, H.; Zhang, X.; Cappa, C. D.; Collier, S.; Zhang, Q.
   Wintertime water-soluble aerosol composition and particle water content in Fresno,
   California. J. Geophys. Res. Atmos. 2017, 122, 3155–3170.
- 616 (43) Graber, E. R.; Rudich, Y. Atmospheric HULIS: How humic-like are they? A comprehensive and critical review. *Atmos. Chem. Phys.* **2006**, *6*, 729–753.
- 618 (44) Tilgner, A.; Schaefer, T.; Alexander, B.; Barth, M.; Collett Jr., J. L.; Fahey, K. M.; Nenes, 619 A.; Pye, H. O. T.; Herrmann, H.; McNeill, V. F. Acidity and the multiphase chemistry of 620 atmospheric aqueous particles and clouds. *Atmos. Chem. Phys.* **2021**, *21*, 13483–13536.
- 621 (45) Buerge-Weirich, D.; Sulzberger, B. Formation of Cu(I) in Estuarine and Marine 622 Waters: Application of a New Solid-Phase Extraction Method To Measure Cu(I). 623 Environ. Sci. Technol. 2004, 38, 1843–1848.
- 624 (46) Deguillaume, L.; Leriche, M.; Desboeufs, K.; Mailhot, G.; George, C.; Chaumerliac, N.
  625 Transition metals in atmospheric liquid phases: sources, reactivity, and sensitive
  626 parameters. *Chem. Rev.* **2005**, *105*, 3388–3431.
- (47) Tapparo, A.; Di Marco, V.; Badocco, D.; D'Aronco, S.; Soldà, L.; Pastore, P.; Mahon, B.
   M.; Kalberer, M.; Giorio, C. Formation of metal-organic ligand complexes affects
   solubility of metals in airborne particles at an urban site in the Po valley. *Chemosphere* 2020, 241, 125025.
- 631 (48) Cheng, Y.; Zheng, G.; Wei, C.; Mu, Q.; Zheng, B.; Wang, Z.; Gao, M.; Zhang, Q.; He, 632 K.; Carmichael, G.; Pöschl, U.; Su, H. Reactive nitrogen chemistry in aerosol water as a 633 source of sulfate during haze events in China. *Sci. Adv.* **2016**, *2*, e1601530.

- 634 (49) Mao, J.; Fan, S.; Jacob, D. J.; Travis, K. R. Radical loss in the atmosphere from Cu-Fe 635 redox coupling in aerosols. *Atmos. Chem. Phys.* **2013**, *13*, 509–519.
- 636 (50) Sannigrahi, P.; Sullivan, A. P.; Weber, R. J.; Ingall, E. D. Characterization of water-637 soluble organic carbon in urban atmospheric aerosols using solid-state 13C NMR 638 spectroscopy. *Environ. Sci. Technol.* **2006**, *40*, 666–672.
- 639 (51) Duarte, R. M. B. O.; Santos, E. B. H.; Pio, C. A.; Duarte, A. C. Comparison of structural 640 features of water-soluble organic matter from atmospheric aerosols with those of aquatic 641 humic substances. *Atmos. Environ.* **2007**, *41*, 8100–8113.
- (52) Huo, Y.; Guo, Z.; Li, Q.; Wu, D.; Ding, X.; Liu, A.; Huang, D.; Qiu, G.; Wu, M.; Zhao,
   Z.; Sun, H.; Song, W.; Li, X.; Chen, Y.; Wu, T.; Chen, J. Chemical fingerprinting of
   HULIS in particulate matters emitted from residential coal and biomass combustion.
   Environ. Sci. Technol. 2021, 55, 3593–3603.
- 646 (53) Richards-Henderson, N. K.; Pham, A. T.; Kirk, B. B.; Anastasio, C. Secondary organic 647 aerosol from aqueous reactions of green leaf volatiles with organic triplet excited states 648 and singlet molecular oxygen. *Environ. Sci. Technol.* **2015**, *49*, 268–276.
- 649 (54) Appiani, E.; Ossola, R.; Latch, D. E.; Erickson, P. R.; McNeill, K. Aqueous singlet 650 oxygen reaction kinetics of furfuryl alcohol: effect of temperature, pH, and salt content. 651 *Environ. Sci.: Processes Impacts* **2017**, *19*, 507–516.
- 652 (55) Bower, J. P.; Anastasio, C. Measuring a 10,000-fold enhancement of singlet molecular oxygen (1O2\*) concentration on illuminated ice relative to the corresponding liquid solution. *Atmos. Environ.* **2013**, *75*, 188–195.
- (56) Smith, J. D.; Kinney, H.; Anastasio, C. Phenolic carbonyls undergo rapid aqueous
   photodegradation to form low-volatility, light-absorbing products. *Atmos. Environ.* 2016,
   126, 36–44.
- Fleming, L. T.; Lin, P.; Roberts, J. M.; Selimovic, V.; Yokelson, R.; Laskin, J.; Laskin,
   A.; Nizkorodov, S. A. Molecular composition and photochemical lifetimes of brown
   carbon chromophores in biomass burning organic aerosol. *Atmos. Chem. Phys.* 2020, 20,
   1105–1129.
- 662 (58) Smith, J. D.; Kinney, H.; Anastasio, C. Aqueous benzene-diols react with an organic 663 triplet excited state and hydroxyl radical to form secondary organic aerosol. *Phys. Chem.* 664 *Chem. Phys.* **2015**, *17*, 10227–10237.
- Wenk, J.; Eustis, S. N.; McNeill, K.; Canonica, S. Quenching of excited triplet states by dissolved natural organic matter. *Environ. Sci. Technol.* **2013**, *47*, 12802–12810.
- 667 (60) Rice-Evans, C. A.; Miller, N. J.; Paganga, G. Structure-antioxidant activity relationships of flavonoids and phenolic acids. *Free Radic. Biol. Med.* **1996**, *20*, 933–956.
- 669 (61) Haag, W. R.; Hoigne', J.; Gassman, E.; Braun, A. Singlet oxygen in surface waters —
  670 Part I: Furfuryl alcohol as a trapping agent. *Chemosphere* **1984**, *13*, 631–640.

- 671 (62) Canonica, S.; Hellrung, B.; Wirz, J. Oxidation of phenols by triplet aromatic ketones in aqueous solution. *The Journal of Physical Chemistry A* **2000**, *104*, 1226–1232.
- (63) Korzeniowska-Sobczuk, A.; Hug, G. L.; Carmichael, I.; Bobrowski, K. Spectral, Kinetics,
   and Theoretical Studies of Radical Cations Derived from Thioanisole and Its Carboxylic
   Derivative. J. Phys. Chem. A 2002, 106, 9251–9260.
- (64) Filipiak, P.; Hug, G. L.; Carmichael, I.; Korzeniowska-Sobczuk, A.; Bobrowski, K.;
   Marciniak, B. Lifetimes and Modes of Decay of Sulfur-Centered Radical Zwitterions
   Containing Carboxylate and Phenyl Groups. J. Phys. Chem. A 2004, 108, 6503–6512.
- 679 (65) Pavitt, A. S.; Bylaska, E. J.; Tratnyek, P. G. Oxidation potentials of phenols and anilines:
   680 correlation analysis of electrochemical and theoretical values. *Environ. Sci. Process.* 681 *Impacts* 2017, 19, 339–349.
- 682 (66) Ohkatsu, Y.; Suzuki, F. Synergism between Phenolic Antioxidants in Autoxidation. *J. Jpn. Petrol. Inst.* **2011**, *54*, 22–29.
- 684 (67) Jørgensen, L. V.; Madsen, H. L.; Thomsen, M. K.; Dragsted, L. O.; Skibsted, L. H. Regeneration of phenolic antioxidants from phenoxyl radicals: an ESR and electrochemical study of antioxidant hierarchy. *Free Radic. Res.* **1999**, *30*, 207–220.
- 687 (68) Fréneau, M.; Hoffmann, N. The Paternò-Büchi reaction—Mechanisms and application to organic synthesis. *J. Photochem. Photobiol. C* **2017**, *33*, 83–108.
- 689 (69) D'Auria, M. The Paternò-Büchi reaction a comprehensive review. *Photochem Photobiol Sci* **2019**, *18*, 2297–2362.
- (70) Aregahegn, K. Z.; Felber, T.; Tilgner, A.; Hoffmann, E. H.; Schaefer, T.; Herrmann, H.
   Kinetics and mechanisms of aqueous-phase reactions of triplet-state imidazole-2-carboxaldehyde and 3,4-dimethoxybenzaldehyde with α,β-unsaturated carbonyl
   compounds. J. Phys. Chem. A 2022, 126, 8727-8740.
- 695 (71) Kaur, R.; Hudson, B. M.; Draper, J.; Tantillo, D. J.; Anastasio, C. Aqueous reactions of 696 organic triplet excited states with atmospheric alkenes. *Atmos. Chem. Phys.* **2019**, *19*, 697 5021–5032.
- 698 (72) Smith, J. D.; Sio, V.; Yu, L.; Zhang, Q.; Anastasio, C. Secondary organic aerosol 699 production from aqueous reactions of atmospheric phenols with an organic triplet excited 700 state. *Environ. Sci. Technol.* **2014**, *48*, 1049–1057.
- 701 (73) Zuo, Y.; Hoigné, J. Evidence for photochemical formation of H2O2 and oxidation of SO2 in authentic fog water. *Science* **1993**, *260*, 71–73.
- 703 (74) Re, R.; Pellegrini, N.; Proteggente, A.; Pannala, A.; Yang, M.; Rice-Evans, C.
   704 Antioxidant activity applying an improved ABTS radical cation decolorization assay.
   705 Free Radic. Biol. Med. 1999, 26, 1231–1237.

- 706 (75) Pellegrini, N.; Del Rio, D.; Colombi, B.; Bianchi, M.; Brighenti, F. Application of the 2,2'-azinobis(3-ethylbenzothiazoline-6-sulfonic acid) radical cation assay to a flow injection system for the evaluation of antioxidant activity of some pure compounds and beverages. *J. Agric. Food Chem.* **2003**, *51*, 260–264.
- 710 (76) Aeschbacher, M.; Graf, C.; Schwarzenbach, R. P.; Sander, M. Antioxidant properties of humic substances. *Environ. Sci. Technol.* **2012**, *46*, 4916–4925.
- 712 (77) Wenk, J.; Aeschbacher, M.; Sander, M.; von Gunten, U.; Canonica, S. Photosensitizing 713 and inhibitory effects of ozonated dissolved organic matter on triplet-induced contaminant 714 transformation. *Environ. Sci. Technol.* **2015**, *49*, 8541–8549.
- 715 (78) Walpen, N.; Houska, J.; Salhi, E.; Sander, M.; von Gunten, U. Quantification of the electron donating capacity and UV absorbance of dissolved organic matter during ozonation of secondary wastewater effluent by an assay and an automated analyzer.

  718 Water Res. 2020, 185, 116235.
- 719 (79) Yuan, Y.; Zhang, H.; Wei, Y.; Si, Y.; Li, G.; Zhang, F. Onsite quantifying electron donating capacity of dissolved organic matter. *Sci. Total Environ.* **2019**, *662*, 57–64.
- 721 (80) Lau, M. P.; Sander, M.; Gelbrecht, J.; Hupfer, M. Solid phases as important electron acceptors in freshwater organic sediments. *Biogeochemistry* **2015**, *123*, 49–61.
- 723 (81) Akherati, A.; He, Y.; Coggon, M. M.; Koss, A. R.; Hodshire, A. L.; Sekimoto, K.;
  724 Warneke, C.; de Gouw, J.; Yee, L.; Seinfeld, J. H.; Onasch, T.B.; Herndon, S.C.;
  725 Knighton, W.B.; Cappa, C.D.; Kleeman, M.J.; Lim, C.Y.; Kroll, J.H.; Pierce, J.R.; Jathar,
  726 S.H. Oxygenated Aromatic Compounds are Important Precursors of Secondary Organic
  727 Aerosol in Biomass-Burning Emissions. *Environ. Sci. Technol.* **2020**, *54*, 8568–8579.
- 728 (82) Bruns, E. A.; El Haddad, I.; Slowik, J. G.; Kilic, D.; Klein, F.; Baltensperger, U.; Prévôt, A. S. H. Identification of significant precursor gases of secondary organic aerosols from residential wood combustion. *Sci. Rep.* **2016**, *6*, 27881.
- 731 (83) McCabe, A. J.; Arnold, W. A. Multiple linear regression models to predict the formation 732 efficiency of triplet excited states of dissolved organic matter in temperate wetlands. 733 *Limnol. Oceanogr.* **2018**, *63*, 1992–2014.
- 734 (84) Chellamani, A.; Sengu, P. Mechanistic study on the oxidation of (phenylthio)acetic acids 735 by oxo(salen)manganese(V) complexes and the reactivity–selectivity principle. *J. Mol.* 736 *Catal. A: Chem* **2008**, *283*, 83–92.
- Liang, Y.; Jen, C. N.; Weber, R. J.; Misztal, P. K.; Goldstein, A. H. Chemical composition of PM<sub>2.5</sub> in October 2017 Northern California wildfire plumes. *Atmos. Chem. Phys.* 2021, *21*, 5719–5737.
- (86) Erickson, P. R.; Moor, K. J.; Werner, J. J.; Latch, D. E.; Arnold, W. A.; McNeill, K.
   Singlet Oxygen Phosphorescence as a Probe for Triplet-State Dissolved Organic Matter
   Reactivity. *Environ. Sci. Technol.* 2018, 52, 9170–9178.

- 743 (87) Schmitt, M.; Erickson, P. R.; McNeill, K. Triplet-State Dissolved Organic Matter
   744 Quantum Yields and Lifetimes from Direct Observation of Aromatic Amine Oxidation.
   745 Environ. Sci. Technol. 2017, 51, 13151–13160.
- 746 (88) Tratnyek, P. G.; Hoigne, J. Oxidation of substituted phenols in the environment: a QSAR 747 analysis of rate constants for reaction with singlet oxygen. *Environ. Sci. Technol.* **1991**, 748 25, 1596–1604.

## Supporting Information for

751

# An Evaluation of Probes to Measure Oxidizing Organic Triplet Excited States in Aerosol Liquid

# Water

Lan Ma, Reed Worland<sup>1</sup>, Theo Tran, and Cort Anastasio\*

Department of Land, Air, and Water Resources, University of California, Davis, CA 95616

Now at Department of Chemistry, University of Washington, Seattle, WA 98195

Correspondence to: Cort Anastasio (canastasio@ucdavis.edu)

This Supporting Information contains 24 pages and includes:

6 sections of text, 11 figures, and 5 tables

/60	Table of Contents
761	Section S1: Chemicals, illumination, and kinetic analysis
762	Section S2. Particle collection and extraction method.
763 764	<b>Section S3:</b> Determination of hydroxyl radical (*OH) and singlet oxygen ( ${}^{1}O_{2}$ *) concentrations in PME.
765	Section S4: Probe inhibition factors and derivation of equation 5
766	Section S5: Determination of second-order rate constant of TPN with <sup>3</sup> DMB*
767	Section S6: Electron donating capacity (EDC) determination
768	Figure S1: Representative plot of decay of TMP and MeJA by <sup>3</sup> BP* with and without SYR+Cu
769	Figure S2: The influence of SYR concentration on the corrected inhibition factor of TMP
770	Figure S3: Inhibition factors of probe compounds in PME5 with 15 μM BP as the triplet precursor 10
771 772	<b>Figure S4:</b> The measured second-order rate constants of TPN reacting with <sup>3</sup> DMB* at pH 2 with different methods
773 774	<b>Figure S5</b> : Absorption spectrum of 50 μM PTA at pH 4.2, the absorbance of 50 μM PTA at 247 nm at different pH, and PTA direct photodegradation rate constant at different pH
775 776	<b>Figure S6</b> : Dependence of first-order PTA decay rate constant on pH for illuminated solutions containing 10 μM DMB and 10 μM PTA
777 778	<b>Figure S7</b> . Dependence of first-order PTA decay rate constant on pH for illuminated solutions containing 15 μM BP and 10 μM PTA
779 780	<b>Figure S8.</b> Bimolecular rate constants for syringol and (phenolthio)acetic acid with the triplet excited states of four model organics
781	Figure S9. Dark reaction of PTA with H <sub>2</sub> O <sub>2</sub>
782 783	<b>Figure S10.</b> Inverse of the PTA first-order decay rate constant with <sup>3</sup> DMB*as a function of the initial PTA concentration at pH 4.2
784 785	<b>Figure S11.</b> Inhibition factor of FFA and PTA, and the corrected inhibition factor of PTA as a function of SYR concentration with BP in SYR+Cu solution at pH 4.2
786	Table S1: The structures of probe compounds.   1
787 788	Table S2. The second-order rate constants of PTA reacting with triplet excited states, singlet oxygen, and hydroxyl radical.
789	Table S3. Characteristic of model triplet species    10
790	Table S4: Summary of inhibition factors of probes with different DOM.    20
791 792	Table S5: PME samples information.    2
793	
794	
, , , ,	

# Section S1. Chemicals, illumination, and kinetic analysis

796

797

798

799

800

801

802

803

804

805

806

807

808

809

810

811

812

813

814

815

816

817

818

819

All chemicals were used as received. Methyl jasmonate (95%), furfuryl alcohol (FFA, 98%), linalool (97%), cis-3-Hexenyl acetate ( $\geq$  98%), prenyl acetate ( $\geq$  98%), atenolol ( $\geq$  98%), (phenylthiol)acetic acid (PTA, 96%), pulegone (≥ 98.5%), syringol (SYR, 99%), benzophenone (BP, 99%), α-terpineol (≥ 96%), 3,4-dimethoxybenzaldehyde (DMB, 99%), Rose Bengal (95%), 2,4,6-trimethylphenol (97%), and 2,2'-azino-bis(3-ethylbenzothiazoline-6-sulfonic acid) diammonium salt (ABTS, ≥ 98%) were from Millipore Sigma. N-cyclopropylaniline (97%) was from Acrotein and 3,5-dichrolo-N-cyclopropylaniline (95%) was from EnamineStore. Suwannee River Fulvic Acid (SRFA) was obtained from the International Humic Substances Society. All chemical solutions were prepared using air-saturated ultrapure water (Milli-Q water) from a Milli-Q Advantage A10 system (Millipore;  $\geq 18.2 \text{ M}\Omega$  cm) with an upstream Barnstead activated carbon cartridge. Solutions were pipetted either into a silicone-plugged GE 021 quartz tube (5 mm inner diameter, 1.0 mL volume) or a 1-cm quartz cuvette (5 mL, Spectrocell). Samples were illuminated at 20 °C with a 1000 W xenon arc lamp filtered with a water filter, an AM1.0 air mass filter (AM1D-3L, Sciencetech), and a 295 nm long-pass filter (20CGA-295, Thorlabs) to simulate tropospheric sunlight. Dark control samples were wrapped in aluminum foil and kept in the photoreactor chamber. During illumination, aliquots were collected from the illuminated and dark cells at specific time intervals to measure concentrations of probes with high-performance liquid chromatography (HPLC, Shimadzu LC-20AB pump, Thermo Scientific Accucore XL C18 column (50 × 3 mm, 4 µm bead), and Shimadzu-M20A UV-Vis detector). The measured pseudo-first-order rate constant for probe loss ( $k'_{Light}$ ) was determined as the negative of the slope from a linear regression of ln([probe]/[probe]<sub>0</sub>) versus illumination time (t), where [probe]<sub>0</sub> is the concentration of probe compound at time zero. The photon flux of the photoreactor was determined on each experiment day by measuring the photolysis rate constant of a 10 µM 2-nitrobenzaldehyde (2NB) solution in the same type of container as that day's sample.<sup>1</sup>

#### Section S2. Particle collection and extraction method

820

821

822

823

824

825

826

827

828

829

830

831

832

833

834

835

836

837

838

Particles were collected on the roof of Ghausi Hall on the UC Davis campus in December 2019, January 2020, and August 2020. In August 2020, there were several wildfires around Davis and air quality was heavily impacted. PM2.5 was collected on Teflon-coated borosilicate glass microfiber filters (Pall Corporation, EmFab<sup>TM</sup> filters, 8 in. × 10 in., pre-cleaned by gently shaking in Milli-Q water and then drying at 100 °C) by a high-volume sampler equipped with a PM<sub>10</sub> inlet (Graseby Andersen) and two offset, slotted impactor plates (Tisch Environmental, Inc., 230 series) to remove particles greater than 2.5 μm. The airflow rate was maintained at 40 (±1) cfm. Particles were either collected for 24 hr or a week. Upon collection, samples were wrapped in aluminum foil (baked previously at 500 °C for 8 hr) and stored at -20 °C. To prepare particulate matter extracts (PMEs), filters were cut into 2 cm × 2 cm pieces, which were each placed in individual 20-mL amber glass vials and extracted with 1.0 mL Milli-Q water by shaking for 4 hr in the dark. The extracts from the same filter were combined, filtered (0.22 µm PTFE; Pall corporation), and adjusted to pH 4.2 using sulfuric acid to mimic the acidity of particle water.<sup>2</sup> PMEs were flash-frozen in liquid nitrogen immediately after preparation and were later thawed on the day of the experiment. Dissolved organic carbon (DOC) and major ion concentrations were measured by a Shimadzu TOC-VCPH analyzer and Metrohm ion chromatographs (881 Compact IC Pro) equipped with conductivity detectors, respectively. PME sample information is provided in Table S5.

839 Section S3. Determination of hydroxyl radical (\*OH) and singlet oxygen (<sup>1</sup>O<sub>2</sub>\*) concentrations in 840 PME

Details about determining  ${}^{\bullet}$ OH and  ${}^{1}$ O<sub>2</sub>\* concentrations are provided in Anastasio et al.<sup>3</sup> and Kaur et al.<sup>4</sup> and are only discussed briefly here. To determine  ${}^{\bullet}$ OH concentrations in PME, we spiked pH-unadjusted 10  $\mu$ M benzoic acid (BA) into PME and illuminated it in a quartz tube, taking aliquots occasionally to measure benzoic acid concentrations by HPLC in order to determine the pseudo-first order decay rate constant for BA loss. The  ${}^{\bullet}$ OH concentration was determined and normalized to sunlight conditions at midday on the winter solstice at Davis (solar zenith =  $62^{\circ}$ ;  $j_{2NB,win} = 0.0070 \, \text{s}^{-1}$ ) and corrected for internal light screening by equation S1:

['OH] = 
$$\left[ \frac{k'_{BA}}{k_{BA+\cdot OH} \times S_{\lambda} \times j_{2NB,exp}} \right] \times j_{2NB,win}$$
 (S1)

where  $k'_{BA}$  is the measured first-order decay rate constant of BA,  $k_{BA+\cdot OH}$  is the second-order rate constant of BA reacting with  ${}^{\bullet}$ OH at pH 4.2 (5.1 × 10<sup>9</sup> M<sup>-1</sup> s<sup>-1</sup>),  ${}^{5,6}$   $S_{\lambda}$  is the internal light screening factor in an individual sample (determined based on the wavelength range 280 – 364 nm), and  $j_{2NB,exp}$  is the photolysis rate constant of 2-nitrobenzaldehyde (2NB) measured on the experiment day.

To determine  ${}^{1}\text{O}_{2}$ \* concentrations, we used FFA as a probe and heavy water (D<sub>2</sub>O) as a diagnostic tool.<sup>3</sup>

We prepared two solutions for each sample: one where 0.5 mL of PME was diluted with 0.5 mL H<sub>2</sub>O and one diluted with 0.5 mL deuterium oxide (D<sub>2</sub>O). We spiked 10 μM FFA into both solutions and determined the loss rate constants of FFA during illumination. The <sup>1</sup>O<sub>2</sub>\* concentration in the undiluted sample was determined from the difference of FFA loss rate constants in H<sub>2</sub>O and D<sub>2</sub>O using equation 14 in Kaur and Anastasio.<sup>7</sup> <sup>1</sup>O<sub>2</sub>\* concentrations were normalized by light screening factors of PME and to Davis winter sunlight, analogous to equation S1.

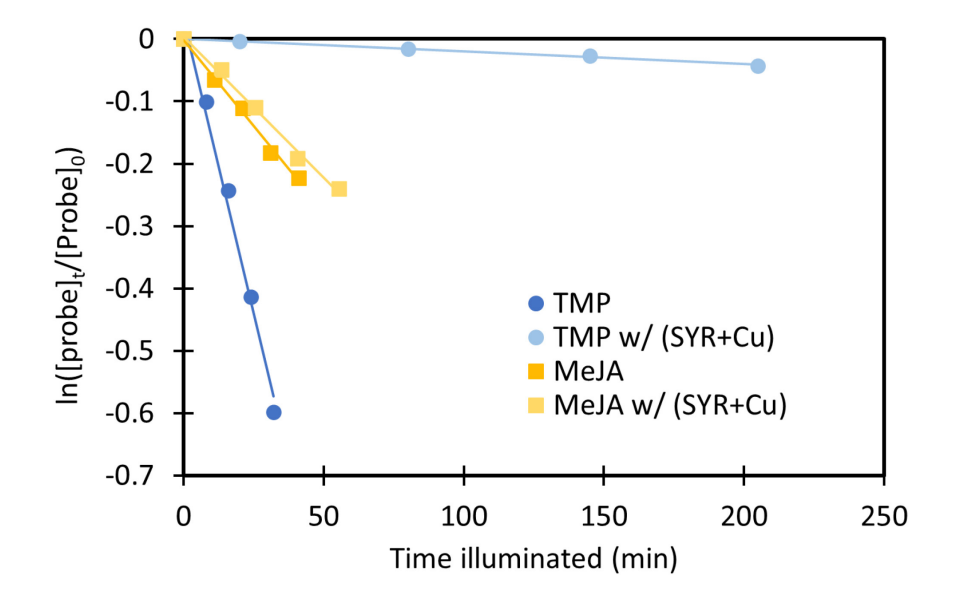
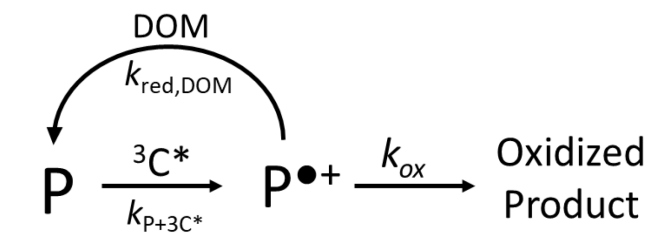


**Figure S1.** Representative plot of decay of TMP and MeJA by the triplet excited state of BP with and without SYR+Cu at pH 4.2. Results shown are for solutions containing 10  $\mu$ M TMP or MeJA, 15  $\mu$ M BP, and with or without 70  $\mu$ M SYR and 1  $\mu$ M Cu(II).

# Section S4: Probe inhibition factors and derivation of equation 5

Scheme 1 shows the kinetic model for reaction of a probe (P) with an oxidizing triplet state (<sup>3</sup>C\*) and the potential inhibition of net probe loss by DOM, as developed by Canonica et al. and Wenk et al. <sup>8,9</sup>



872

869

Scheme S1

- The probe (P) is oxidized by  ${}^{3}C^{*}$  with a rate constant  $k_{P+3C^{*}}$  to form the intermediate radical cation (P $^{\bullet+}$ ).
- The intermediate can either undergo further oxidation to form oxidized product with first-order rate
- constant  $k_{ox}$ , or be reduced by DOM back to P with a second-order rate constant  $k_{red,DOM}$ .
- 877 In addition to regenerating oxidized probe, DOM can also reduce net probe loss by acting as a sink for
- 878 triplets, decreasing the steady-state concentration of <sup>3</sup>C\*. We can quantify this suppression of triplet
- concentration by DOM with the inhibition factor for FFA loss ( $IF_{FFA}$ ). Since the  ${}^{1}O_{2}$ \* concentration is
- proportional to total  ${}^{3}C^{*}$ ,  $IF_{FFA}$  can be expressed as

881 
$$IF_{FFA} = \frac{[{}^{3}C^{*}]_{DOM}}{[{}^{3}C^{*}]_{0}}$$
 (S2)

- where [<sup>3</sup>C\*]<sub>DOM</sub> is the triplet concentration in the presence of DOM (or SYR+Cu), and [<sup>3</sup>C\*]<sub>0</sub> is the triplet
- concentration without DOM or SYR+Cu. In the absence of DOM or SYR+Cu, the pseudo-first-order
- decay rate constant of triplet probe by <sup>3</sup>C\* can be expressed as:

$$k'_{p,0} = k_{P+3C*}[^{3}C^{*}]_{0}$$
 (S3)

- In the presence of DOM or SYR+Cu, the decay rate of the probe by <sup>3</sup>C\* can be expressed with the
- 887 equation below from Wenk et al.:9

888 
$$k'_{p,DOM} = k_{P+3C*}[^{3}C^{*}]_{DOM} \left(\frac{k_{ox}}{k_{ox} + k_{red,DOM}[DOM]}\right)$$
(S4)

- where the factor in parentheses represents the fraction of  $P^{\bullet +}$  that is oxidized to stable product rather than
- reduced back to P. Based on this, the inhibition factor for the probe  $(IF_P)$ , can be expressed as a function
- 891 of  $IF_{FFA}$ :

892 
$$IF_{P} = \frac{k'_{P,DOM}}{k'_{P,0}} = \frac{k_{P+3C*}[^{3}C^{*}]_{DOM}(\frac{k_{ox}}{k_{ox} + k_{red,DOM}[DOM]})}{k_{P+3C*}[^{3}C^{*}]_{0}} = IF_{FFA}\left(\frac{k_{ox}}{k_{ox} + k_{red,DOM}[DOM]}\right) \quad (S5)$$

The inhibition factor  $IF_P$  includes both of the impacts of DOM on probe loss, i.e., the decrease in  ${}^3C^*$  concentration and regeneration of oxidized probe back to its original state. We define  $IF_{P,corr}$  as the corrected inhibition factor, which only expresses the inhibition effect of DOM on  $P^{\bullet +}$ :

$$IF_{P,corr} = \left(\frac{k_{ox}}{k_{ox} + k_{red,DOM}[DOM]}\right) = \frac{IF_P}{IF_{FFA}}$$
 (S6)

A value of  $IF_{FFA}$  greater than 1 indicates DOM is not appreciably suppressing the  ${}^{3}C^{*}$  concentration. Under this condition, we assume  $IF_{P,corr} = IF_{P}$ . A value of  $IF_{P}$  above 1 indicates no suppression of probe loss by sample components (e.g., DOM or SYR + Cu). Under this condition we assume  $IF_{P,corr} = IF_{P}$ , and we do not make a correction for the  ${}^{3}C^{*}$  concentration. The four cases for values of  $IF_{P}$  and  $IF_{FFA}$  are shown in the table below: the entry for each pair of values shows how the corresponding value of  $IF_{P,corr}$ was calculated.

	$IF_P \leq 1$	$IF_P > 1$
$IF_{FFA} \leq 1$	IF <sub>P</sub> / IF <sub>FFA</sub>	IF <sub>P</sub> <sup>a</sup>
$IF_{FFA} > 1$	$IF_P$	IF <sub>P</sub> <sup>a</sup>

a While we report  $\overline{IF_{P,corr}} = \overline{IF_P}$  for samples when  $\overline{IF_P} > 1$ , we do not make a correction for the  ${}^3C^*$  concentration when  $\overline{IF_{P,corr}} > 1$ , i.e., we use  $[{}^3C^*]_{P,corr} = [{}^3C^*]_P$ .

We can also derive an equation for the inhibition factor of FFA due to triplet quenching. In equation S2, [<sup>3</sup>C\*]<sub>DOM</sub> and [<sup>3</sup>C\*]<sub>0</sub> can be expressed as

907 
$$[^{3}C^{*}]_{DOM} = \frac{P_{3C*}}{k'_{O2} + k_{DOM+3C*}[DOM]}$$
 (S7)

where  $P_{3C^*}$  is the rate of  ${}^3C^*$  formation,  $k'_{O2}$  is the pseudo-first-order rate constant of dissolved oxygen quenching  ${}^3C^*$ , which is a constant, and  $k_{DOM+3C^*}$  is the second-order rate constant of DOM quenching  ${}^3C^*$ . Therefore,  $IF_{FFA}$  can be expressed as

912 
$$IF_{FFA} = \frac{\frac{P_{3C*}}{k'_{O2} + k_{DOM+3C*}[DOM]}}{\frac{P_{3C*}}{k'_{O2}}} = \frac{k'_{O2}}{k'_{O2} + k_{DOM+3C*}[DOM]}$$
(S9)

Taking the inverse of equation S9, we obtain:

914 
$$\frac{1}{IF_{FFA}} = 1 + \frac{k_{DOM+3C*}}{k'_{O2}}[DOM]$$
 (S10)

This equation has the same functional form as equation 7 in the main text but the fitted parameters here have different physical meanings.

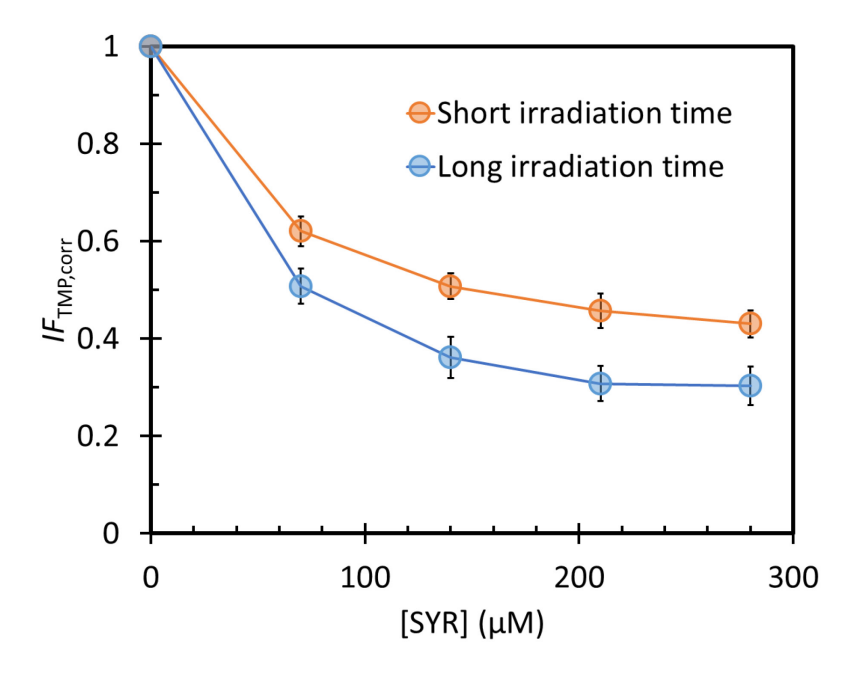


**Figure S2**. Influence of SYR on the decay of TMP by  ${}^{3}$ BP\*, shown as the corrected inhibition factor of TMP. Since the TMP decay at each SYR concentration was not strictly first order, with TMP decays faster at short irradiation times, we calculated  $IF_{TMP,corr}$  with both the short- and long-time kinetic data. Solutions contained 10  $\mu$ M TMP, 15  $\mu$ M BP, and 0 to 280  $\mu$ M syringol. No Cu(II) was added.

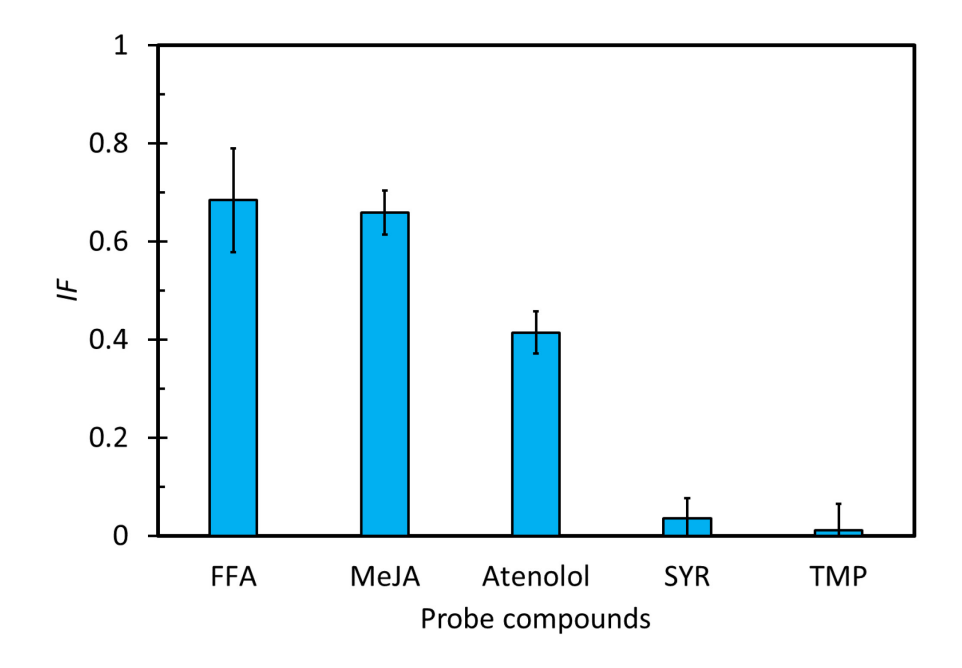


Figure S3. Inhibition factors of probe compounds in PME5 with 15  $\mu$ M BP as the triplet precursor. Data are shown in Table S3. Error bars represent  $\pm 1$  standard error propagated from the linear regression.

**Table S1.** The structures of probe compounds in Table 1

Classes	Compounds	Structure	р $K_a$
Sulfide	(Phenylthio)acetic acid (PTA)	s OH	3.56 <sup>a</sup>
	Methyl jasmonate (MeJA)	O OCH <sub>3</sub>	
	Terpineol (TPN)	OH CH <sub>3</sub> CH <sub>3</sub>	
Alkenes	Pulegone	H <sub>3</sub> C - CH <sub>3</sub>	
	cis-3-Hexenyl acetate	H <sub>3</sub> C CH <sub>3</sub>	
	Prenyl acetate	O CH <sub>3</sub>	
	Linalool	НО	
Amine	Atenolol (ANL)	O O O O O O O O O O O O O O O O O O O	9.6 <sup>b10</sup>
	N-cyclopropylaniline (CAN)	N N	~4.6 <sup>c11</sup>
Anilines	3,5-dichloro- <i>N</i> -cyclopropylaniline (DCCAN)	CI	
	Syringol (SYR)	H <sub>3</sub> CO OCH <sub>3</sub>	~10.0 <sup>d12</sup>
Phenols <sup>a</sup> In thi	2,4,6-trimethylphenol (TMP)	OH CH <sub>3</sub> CH <sub>3</sub>	10.913

<sup>&</sup>lt;sup>a</sup> In this work. <sup>b</sup>  $pK_a$  of atenolol with protonated nitrogen <sup>c</sup>  $pK_a$  value of protonated aniline. <sup>d</sup>  $pK_a$  value of guaiacol (2-methoxyphenol).

### Section S5. Determination of the second-order rate constant of TPN with <sup>3</sup>DMB\*

936

937

938939

940

941

942

943944

945

946

947

948

949

950

951

952

953954

955

956

The photochemical reaction between a carbonyl compound and an alkene can form an oxetane through the Paternò-Büchi reaction. 14,15 This is a photocyloaddition between an excited carbonyl compound (singlet or triplet state) and an alkene. The mechanism can either form a diradical intermediate or an exciplex from charge-transfer complexes. The latter involves intermolecular electron transfer to form a radical-ion pair, which is observed only for very electron-rich alkenes. <sup>16</sup> The mechanistic pathway depends on the difference in redox potentials between the alkene and the singlet or triplet state of the carbonyl compound. <sup>17</sup> If the redox potential of alkene is smaller, electron transfer might proceed. Therefore, the reaction between alkene and triplets does not necessarily involve electron transfer, complicating the use of alkenes to determine concentrations of oxidizing triplets. Consequently, alkenes do not appear to be appropriate as probes for oxidizing triplets, although alkene decay is not inhibited by DOM, which is likely a consequence of the irreversible formation of oxetane. Prior to recognizing the Paternò-Büchi reaction, we worked to assess alkenes as oxidizing triplet probes because of their resistance to inhibition. We encountered difficulty determining the bimolecular rate constant of  $\alpha$ -terpineol with <sup>3</sup>DMB\*. As shown in Figure S4, our measured values are different with different methods. The red triangles represent rate constants obtained with a direct measurement technique described in Smith et al. and Ma et al. 18,19 The values of the rate constant vary by a factor of 2.5 between the two measurements. Also, when using a relative rate method, the TPN concentration appears to affect the TPN rate constant: rate constants determined with 10 µM TPN are about 4 times lower than those measured with 20 µM TPN.

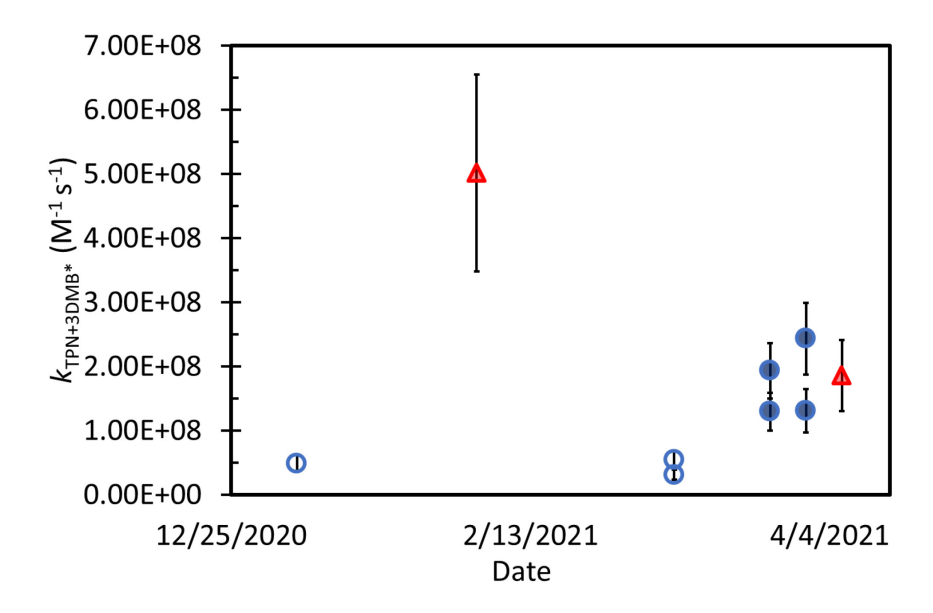


**Figure S4.** Measured second-order rate constants of TPN reacting with  $^3DMB^*$  at pH 2 with two different experimental methods. The red triangles represent values obtained with a direct measurement method.  $^{20}$  The open blue circles represent values from a relative rate method using 10  $\mu$ M TPN, while the solid blue circles represent the values obtained using 20  $\mu$ M TPN.

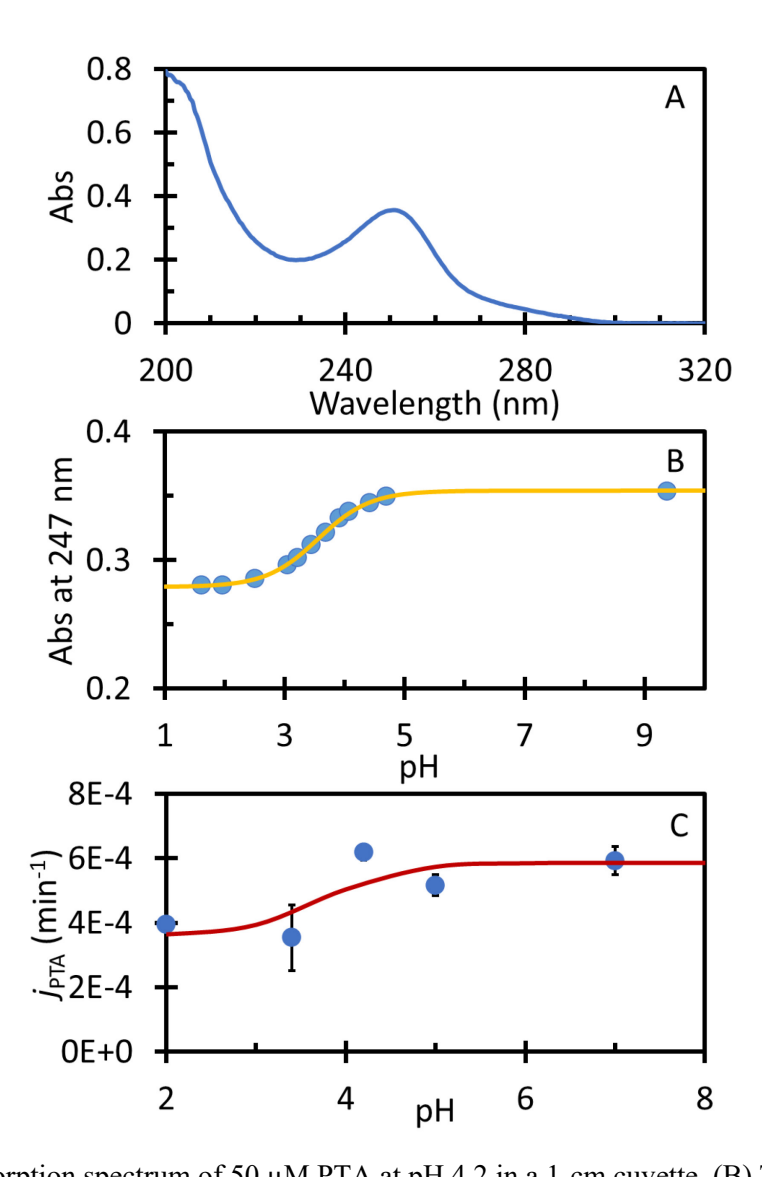
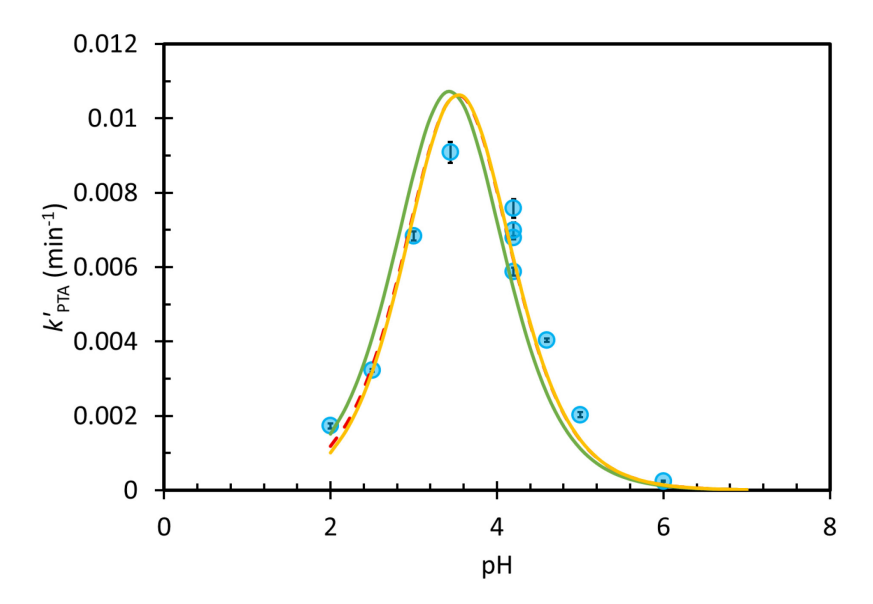
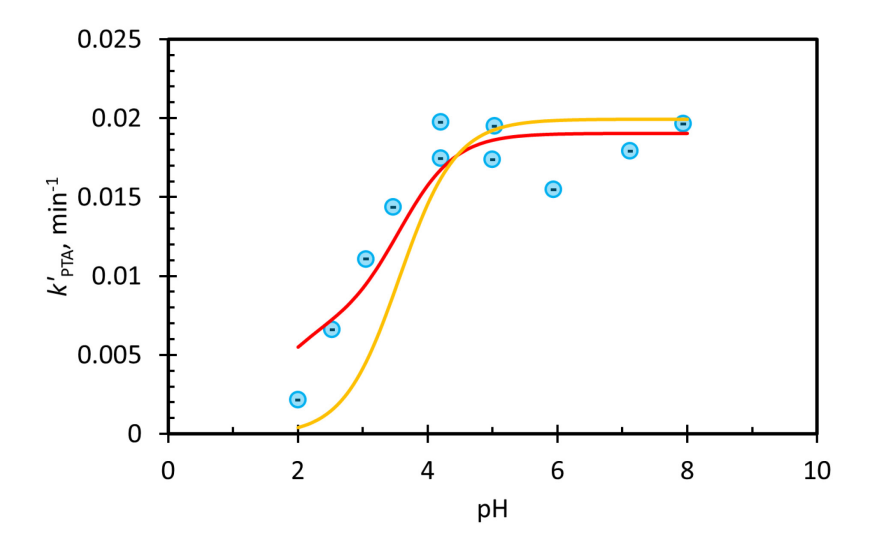


Figure S5. (A) Absorption spectrum of 50 μM PTA at pH 4.2 in a 1-cm cuvette. (B) The absorbance of 50 μM PTA solution at 247 nm as a function of pH in a 1-cm cuvette. Data are fitted with the equation  $Abs_{TOT} = Abs_{HPTA} + \frac{Abs_{PTA} - Abs_{HPTA}}{1 + \frac{[H^+]}{Ka}}$  to obtain p $K_a$ ,  $Abs_{PTA}$  and  $Abs_{HPTA}$  values, where  $Abs_{TOT}$  is the absorbance of a 50 μM PTA solution (in a 1-cm cell) at 247 nm at different pH values,  $Abs_{HPTA}$  and  $Abs_{PTA}$  are the absorbance values of the protonated and deprotonated forms of PTA, respectively. From the fitting, p $K_a = 3.56 \pm 0.02$ ,  $Abs_{HPTA} = 0.28 \pm 0.01$  and  $Abs_{PTA} = 0.35 \pm 0.01$ . (C) Winter solstice-normalized direct photodegradation rate constant of PTA as a function of pH. Data are fitted with the equation  $j_{TOT} = j_{HPTA} + \frac{j_{PTA} - j_{HPTA}}{1 + \frac{[H^+]}{Ka}}$  to  $j_{HPTA}$  and  $j_{PTA}$  values, which are direct photodegradation rate constants of protonated and deprotonated forms of PTA, respectively. From the fitting,  $j_{HPTA} = 3.5 \pm 0.7$  ×10<sup>-4</sup> min<sup>-1</sup> and  $j_{PTA} = 5.8 \pm 0.5$  ×10<sup>-4</sup> min<sup>-1</sup>.



**Figure S6.** Dependence of the measured first-order PTA decay rate constant on pH for illuminated solutions containing 10  $\mu$ M DMB and 10  $\mu$ M PTA at 20 °C. The red dashed line is the regression in Figure 2. The green solid line represents the regression fit to eq 6 using 3.3 as the p $K_a$  of <sup>3</sup>DMB\*, with a, b, and d set as zero and the fitted c value of 0.059 min<sup>-1</sup> The yellow solid line represents the regression fit with b and d set to zero, with fitted a and c values of -1.9 ×10<sup>-4</sup> min<sup>-1</sup> and 0.046 min<sup>-1</sup>, respectively.



**Figure S7.** pH dependence of the first-order PTA decay rate constant for illuminated solutions containing 15  $\mu$ M BP and 10  $\mu$ M PTA at 20 °C. The red line is the regression fitted to a BP-analog of eq 6, with a and c set to zero and fitted b and d values of 0.0069 min<sup>-1</sup> and 0.19 min<sup>-1</sup>, respectively. The yellow line represents the regression fit with a, b, and c set as zero and a fitted d value of 0.020 min<sup>-1</sup>. We used the  ${}^{3}$ BP\*  $pK_{a}$  of 1.5 in all regression fits. ${}^{21}$ 

**Table S2.** Second-order rate constants of PTA reacting with triplet excited states, singlet oxygen, and hydroxyl radical.

	Rate constant at pH 4.2 (M <sup>-1</sup> s <sup>-1</sup> )	Method (Reference compound)	Reference compound rate constant	Reference for reference compound rate constant
k <sub>PTA+3BP*</sub>	$5.0 (\pm 0.9) \times 10^9$	Relative (TMP)	$5.1 (\pm 0.9) \times 10^9$	Canonica et al. <sup>13</sup>
$k_{PTA+3DMB}\ast$	2.5 (±0.6) ×10 <sup>9</sup>	Direct <sup>a</sup>	-	
$k_{PTA+3MAP^{\ast}}$	$3.1 (\pm 0.4) \times 10^9$	Relative (TMP)	$2.6 (\pm 0.3) \times 10^9$	Canonica et al. <sup>13</sup>
$k_{PTA+2AN^{\ast}}$	$2.4 (\pm 0.2) \times 10^{7}$	Relative (TMP)	$7.2 (\pm 0.1) \times 10^{8}$	Canonica et al. <sup>13</sup>
$k_{PTA+1O2}\ast$	$8.8 (\pm 0.6) \times 10^6$	Relative (FFA)	$1.0 (\pm 0.1) \times 10^{8}$	Appiani et al. <sup>22</sup>
$k_{PTA+OH}\ast$	$10.3 (\pm 0.6) \times 10^9$	Relative (Benzene)	$7.7 (\pm 0.4) \times 10^9$	Kochany et al. <sup>23</sup>

<sup>&</sup>lt;sup>a</sup> See Figure S9

992

993

994

995

996 997

998 999

989

991 **Table S3.** Characteristic of model triplet species

Model Triplet	E <sub>T</sub> (kJ mol <sup>-1</sup> ) <sup>a</sup>	$E_0*(^3C*/C^{\bullet-})(V)^b$	pK <sub>a</sub> <sup>c</sup>
2-acetonaphthone ( <sup>3</sup> 2AN*)	249	1.10	
3-methoxyacetophenone	303	1.64	
$(^{3}3MAP*)$			
3,4-dimethoxybenzaldehyde	268	-	3.3 <sup>d</sup>
( <sup>3</sup> DMB*)			
Benzophenone ( <sup>3</sup> BP*)	288	1.69	1.5 <sup>e</sup>

All values are from Canonica et al. and Felber et al. unless noted<sup>13,24</sup>

<sup>&</sup>lt;sup>a</sup> Triplet state energy  $(T_1 \rightarrow S_0)$ 

<sup>&</sup>lt;sup>b</sup>One-electron reduction potential for the triplet/triplet radical anion pair

<sup>&</sup>lt;sup>c</sup> Acid dissociation constant of the protonated triplet state

<sup>&</sup>lt;sup>d</sup> Reference 20<sup>20</sup>

<sup>&</sup>lt;sup>e</sup> Reference 21<sup>21</sup>

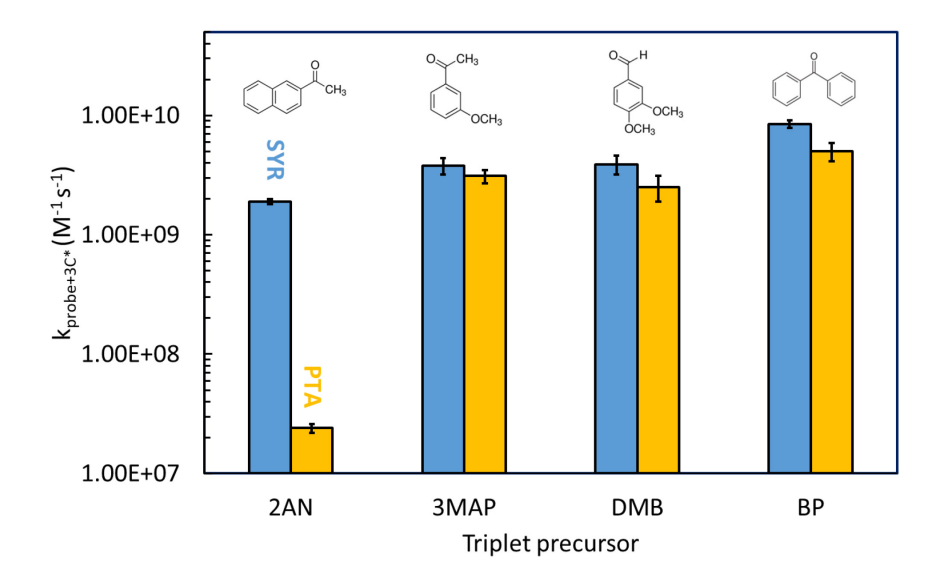


**Figure S8.** Bimolecular rate constants for syringol (blue) and (phenolthio)acetic acid (yellow) with the triplet excited states of four model organics. Structures show the ground state of each photosensitizer.

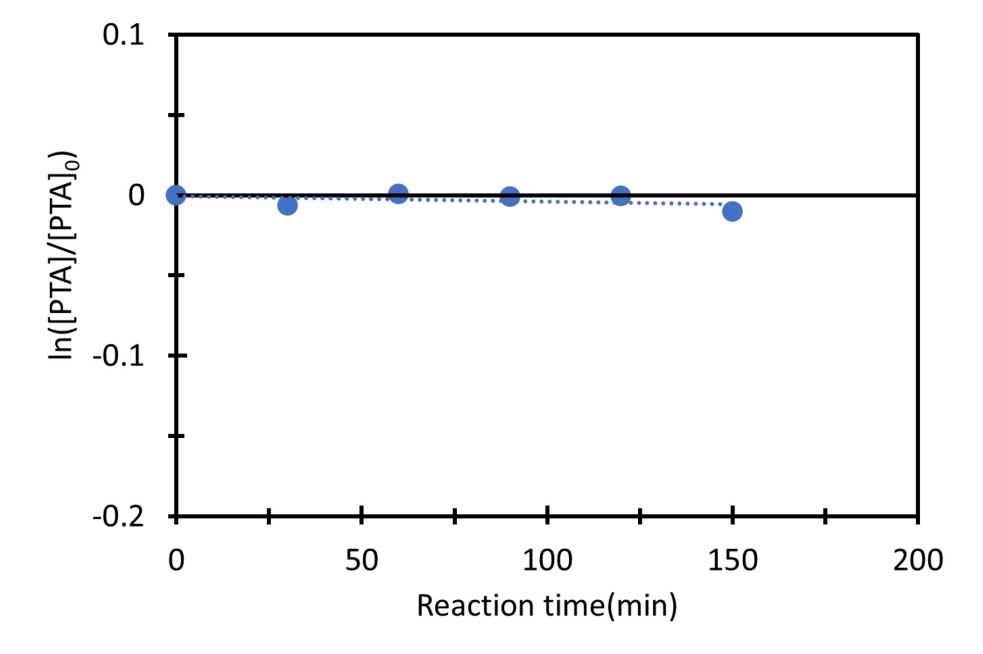
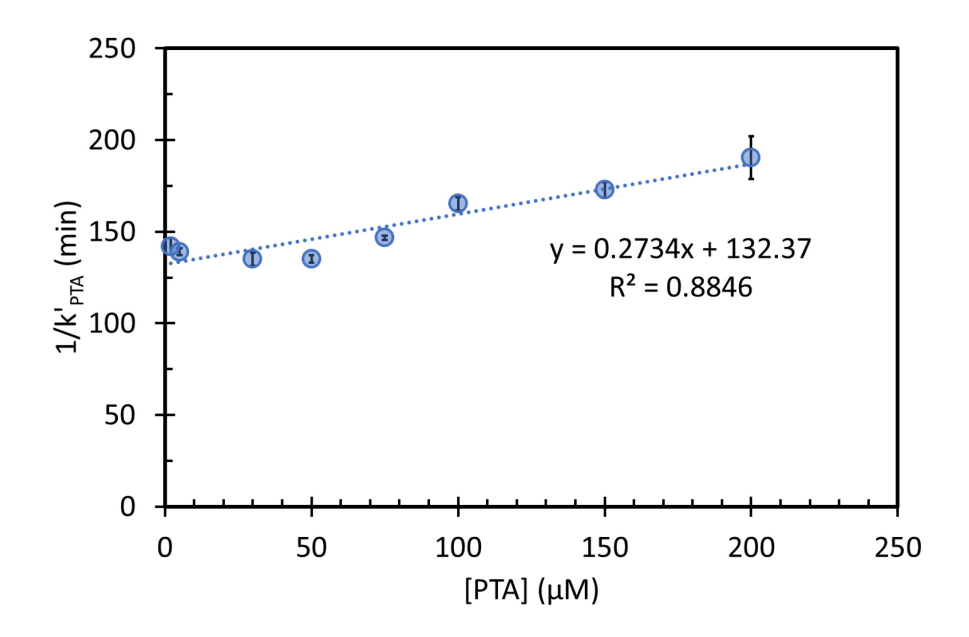
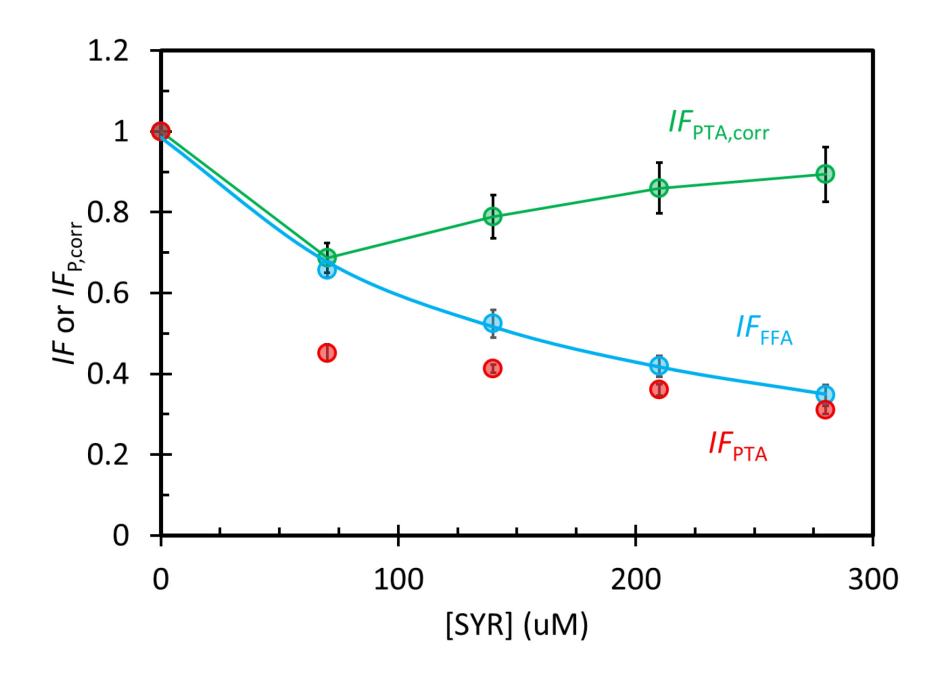


Figure S9. The dark reaction of 20  $\mu$ M PTA and 100  $\mu$ M H<sub>2</sub>O<sub>2</sub> at pH 4.2. The PTA loss is less than 2%, which is negligible compared to PTA loss in corresponding experiments with triplets.



**Figure S10.** Inverse of the PTA first-order decay rate constant with  ${}^{3}DMB^{*}$  as a function of initial PTA concentration at pH 4.2. The dotted line is a linear regression fit to the data. Error bars on points represent  $\pm$  1 standard error propagated from the errors of  $k'_{PTA}$  and  $j_{PTA}$ . Details of the method to determine  $k_{PTA+3DMB^{*}}$  are provided in Smith et al. and Ma et al.  ${}^{19,20}$ 

### 1014 Section S6. Electron Donating Capacity (EDC) Determination We adapted the EDC method from Walpen et al. and Yuan et al. 25,26, using a 0.10 mM ABTS (2,2'-azino-1015 1016 bis(3-ethylbenzothiazoline-6-sulfonic acid) solution prepared with acetate buffer (0.05 M) to maintain pH 1017 at 4.2. We prepared a 10 mM NaClO solution by diluting concentrated sodium hypochlorite solution using the molar absorption coefficient of hypochlorite ( $\varepsilon(292 \text{ nm}) = 359 \text{ M}^{-1}\text{cm}^{-1}$ at pH 11).<sup>27</sup> The 1018 1019 ABTS<sup>•+</sup> solution was prepared by adding 10 mM NaClO to ABTS solution to oxidize around 70% of the ABTS to ABTS<sup>•+</sup>, and then shaking for 10 min. To determine EDC for PME, 200 μL PME (for extracts 1020 with high DOC) or 1 ml PME (for extracts with low DOC) was spiked into 5.0 mL of ABTS<sup>•+</sup> solution. 1021 1022 After spiking, we shook the solution for 5 min and then let it stand for 10 min. The absorbance of the 1023 solution at 728 nm was measured by a UV-Vis spectrophotometer to determine the ABTS<sup>•+</sup> concentration (using a molar absorption coefficient $\varepsilon = 14000 \text{ M}^{-1} \text{ cm}^{-1}$ at 728 nm)<sup>28</sup> and EDC was determined from a 1024 standard curve prepared using Trolox. 1025 1026



**Figure S11.** Inhibition factors of FFA (blue) and PTA (red), and the corrected inhibition factor of PTA (green), as a function of SYR concentration with 15  $\mu$ M BP as the triplet precursor in SYR+Cu solution at pH 4.2. The red and blue lines were determined from linear regressions between the inverse of *IF* values versus the SYR concentration. Error bars represent  $\pm 1$  SE, propagated from the linear regression.

Table S4. Summary of inhibition factors of probes with different DOM

		PME1	PME2	PME3	PME4	PME5 <sup>b</sup>	SRFA	SRFA	70 μM SYR + 1 μM Cu(II)	140 μM SYR + 2 μM Cu(II)	210 μM SYR + 3 μM Cu(II)	280 μM SYR + 4 μM Cu(II)	350 μM SYR + 5 μM Cu(II)	420 μM SYR + 6 μM Cu(II)
DOC (mg C L <sup>-1</sup> )		9.9	63.7	68.8	104.9	27.8	25.8	51.5	6.7	13.4	20.2	26.9	33.6	40.3
EDO (mmol e	$g_{\rm C}^{-1}$	< LOD <sup>a</sup>	1.8 (±0.1)	1.7 (±0.2)	4.4 (±0.1)	-	1.7 (±0.1)	1.7 (±0.1)	36	28	28	27	29	29
EDC×I			0.11	0.12	0.47	_		0.08						
(mmol e	- L-1)	< LOD	(±0.01)	$(\pm 0.01)$	$(\pm 0.01)$		0.04 (±0.01)	$(\pm 0.02)$	0.25	0.38	0.56	0.73	0.96	1.16
	FFA	1.10 (±0.07)	1.00 (±0.20)	1.30 (±0.12)	1.00 (±0.12)	-	1.91 (±0.14)	-	0.83 (±0.04)	0.77 (±0.04)	0.56 (±0.04)	0.55 (±0.04)	0.50 (±0.10)	0.44 (±0.03)
<i>IF</i> w/ 80 μM DMB	SYR	$0.76 \ (\pm 0.03)$	0.48 (±0.03)	0.21 (±0.04)	0.31 (±0.02)	-	1.17 (±0.10)	-	-	-	-	-	-	_
	PTA	0.75 (±0.03)	1.24 (±0.06)	1.26 (±0.03)	$0.60 \ (\pm 0.04)$	-	0.83 (±0.05)		0.74 (±0.01)	0.54 (±0.01)	0.44 (±0.01)	0.35 (±0.01)	0.27 (±0.01)	0.23 (±0.01)
	FFA	-	-	-	-	0.68 (±0.10)	-	0.71 (±0.32)	0.66 (±0.02)	0.52 (±0.03)	0.42 (±0.03)	0.35 (±0.02)	-	-
	SYR	-	-	-	-	0.03 (±0.04)	-	0.61 (±0.11)	-	-	-	-	-	-
	PTA	-	-	-	-	-	-	-	0.45 (±0.02)	0.41 (±0.01)	0.36 (±0.01)	0.31 (±0.10)	-	-
<i>IF</i> w/ 15 μM BP	TMP	-	-	-	-	0.01 (±0.05)	-	-	0.01 (±0.01)	-	-	-	-	-
	Aten- olol	-	-	-	-	0.41 (±0.04)	-	-	-	-	-	-	-	-
	MeJA	-	-	-	-	0.66 (±0.04)	-	0.47 (±0.02)	0.71 (±0.05)	0.49 (±0.01)	0.41 (±0.01)	-	-	-
	TPN	-	-	-	-	-	-	-	0.65 (±0.01)	0.49 (±0.01)	0.43 (±0.01)	0.35 (±0.01)	-	-

Errors (in parentheses) represent one standard error propagated from the error of linear regression.

<sup>&</sup>lt;sup>a</sup> Below detection limit.

<sup>&</sup>lt;sup>b</sup> PME5 was used to determine *IF* values with BP but was not characterized for photooxidant concentrations.

**Table S5. Information on PME samples** 

Sample ID	PME1	PME2	PME3	PME4	PME5 <sup>g</sup>
~ 44			10/10/10/10/10		01/10/16 -
Collection dates	08/04/20 - 08/21/20	01/03/20 - 01/10/20			01/12/16
Collection time (hr)	24	168 (one week)	168 (one week)	24	28
Daily PM <sub>2.5</sub> concentration					
$(\mu g m^{-3}-air)^a$	6.9	9.0	10	50	5.9
Average mass of PM					
extracted (µg) <sup>b</sup>	79 (±14)	620 (±53)	540 (±35)	311 (±21)	132 (±11)
PM mass/water ratio					
$(10^{-4} \mu g PM/\mu g H_2O)$	$0.79 (\pm 0.14)$	6.2 (±0.5)	5.4 (±0.4)	3.1 (±0.2)	1.3 (±0.1)
$\alpha_{300}  (\text{cm}^{-1})^{\text{c}}$	0.020	0.553	0.723	1.524	0.33
AAE (300-450) <sup>d</sup>	6.7	7.7	7.4	7.4	6.2
DOC (mg C L <sup>-1</sup> )	9.9	63.7	68.8	104.9	27.8
EDC (mmol e <sup>-</sup> L <sup>-1</sup> )	< LODe	0.11 (±0.01)	0.12 (±0.01)	$0.47 (\pm 0.01)$	-
$[^{1}O_{2}^{*}] (10^{-12} \text{ M})$	$0.080 (\pm 0.003)$	2.3 (±0.1)	2.5 (±0.2)	3.0 (±0.2)	-
$[OH] (10^{-15} M)$	$0.23~(\pm 0.03)$	4.7 (±0.3)	3.9 (±0.3)	2.0 (±0.4)	-
$I\!F_{ ext{FFA}}{}^{ ext{f}}$	$1.10 (\pm 0.07)$	0.97 (±0.20)	1.30 (±0.12)	1.00 (±0.12)	-
$IF_{\mathrm{SYR}}{}^{\mathrm{f}}$	$0.76 (\pm 0.03)$	$0.48 (\pm 0.03)$	0.21 (±0.04)	0.31 (±0.02)	-
$IF_{ m SYR,corr}$	$0.76~(\pm 0.03)$	$0.49 (\pm 0.11)$	0.21 (±0.04)	$0.31 (\pm 0.02)$	-
$IF_{PTA}{}^{\mathrm{f}}$	0.75 (±0.03)	1.24 (±0.06)	1.26 (±0.03)	$0.60~(\pm 0.04)$	-
$IF_{ m PTA,corr}$	$0.75 (\pm 0.03)$	1.24 (±0.06)	1.26 (±0.03)	$0.60 (\pm 0.04)$	-
$[^{3}C^{*}]_{SYR} (10^{-14} M)$	0.66 (±0.15)	9.3 (±1.9)	9.4 (±2.2)	20 (±5)	-
$[^{3}C^{*}]_{SYR,corr} (10^{-14} \text{ M})$	0.87 (±0.20)	19 (±6)	45 (±13)	64 (±16)	-
$[^{3}C^{*}]_{PTA} (10^{-14} M)$	0.21 (±0.09)	21 (±5)	20 (±5)	10 (±3)	-
[ <sup>3</sup> C*] <sub>PTA,corr</sub> (10 <sup>-14</sup> M)	0.28 (±0.12)	21 (±5)	20 (±5)	17 (±4)	-

<sup>&</sup>lt;sup>a</sup> Daily PM<sub>2.5</sub> concentration for each sampling period measured at the UC Davis sampling site by the

California Air Resources as reported on the *i*ADAM online database (California Air Resources Board, 2019 –2020)

<sup>1040</sup> b The average ( $\pm 1\sigma$ ) mass of PM extracted from each 2 cm  $\times$  2 cm filter square.

<sup>1041 &</sup>lt;sup>c</sup> Base-10 absorbance coefficient of the extract (in cm<sup>-1</sup>) at 300 nm.

d Absorption Angstrom Exponent (AAE) describes the dependence of absorbance on wavelength from 300 nm to 450 nm and is calculated with equation: AAE = [log(Abs<sub>300</sub>) – log(Abs<sub>450</sub>)]/log(300/450), where Abs<sub>450</sub> and Abs<sub>300</sub> are the absorbances at 450 and 300 nm, respectively.

<sup>1045 &</sup>lt;sup>e</sup> Below detection limit.

 $<sup>^{1046}</sup>$   $^{f}$  IF values shown in this table were measured with 80  $\mu$ M DMB.

g PME5 was prepared using a particle filter collected by Kaur et al.<sup>29</sup> PME5 was used to determine *IF* values with BP but was not characterized for photooxidant concentrations.

## 1050 REFERENCES

- 1051 (1) Galbavy, E. S.; Ram, K.; Anastasio, C. 2-Nitrobenzaldehyde as a chemical actinometer for solution and ice photochemistry. *J. Photochem. Photobiol. A* **2010**, *209*, 186–192.
- 1053 (2) Parworth, C. L.; Young, D. E.; Kim, H.; Zhang, X.; Cappa, C. D.; Collier, S.; Zhang, Q.
  1054 Wintertime water-soluble aerosol composition and particle water content in Fresno, California. *J. Geophys. Res. Atmos.* **2017**, *122*, 3155–3170.
- 1056 (3) Anastasio, C.; McGregor, K. G. Chemistry of fog waters in California's Central Valley: 1. In situ photoformation of hydroxyl radical and singlet molecular oxygen. *Atmos. Environ.* **2001**, *35*, 1058 1079–1089.
- 1059 (4) Kaur, R.; Anastasio, C. First measurements of organic triplet excited states in atmospheric waters. 1060 Environ. Sci. Technol. 2018, 52, 5218–5226.
- 1061 (5) Ashton, L.; Buxton, G. V.; Stuart, C. R. Temperature dependence of the rate of reaction of OH with some aromatic compounds in aqueous solution. Evidence for the formation of a π-complex intermediate? J. Chem. Soc., Faraday Trans. 1995, 91, 1631–1633.
- Wander, R.; Neta, P.; Dorfman, L. M. Pulse radiolysis studies. XII. Kinetics and spectra of the cyclohexadienyl radicals in aqueous benzoic acid solution. *J. Phys. Chem.* **1968**, *72*, 2946–2949.
- 1066 (7) Kaur, R.; Anastasio, C. Light absorption and the photoformation of hydroxyl radical and singlet oxygen in fog waters. *Atmos. Environ.* **2017**, *164*, 387–397.
- 1068 (8) Canonica, S.; Laubscher, H.-U. Inhibitory effect of dissolved organic matter on triplet-induced oxidation of aquatic contaminants. *Photochem. Photobiol. Sci.* **2008**, *7*, 547.
- Wenk, J.; von Gunten, U.; Canonica, S. Effect of dissolved organic matter on the transformation of contaminants induced by excited triplet states and the hydroxyl radical. *Environ. Sci. Technol.* **2011**, *45*, 1334–1340.
- 1073 (10) Martínez, V.; Maguregui, M. I.; Jiménez, R. M.; Alonso, R. M. Determination of the pKa values of β-blockers by automated potentiometric titrations. *J. Pharm. Biomed. Anal.* **2000**, *23*, 459–468.
- 1075 (11) Gross, K. C.; Seybold, P. G. Substituent effects on the physical properties and pKa of aniline. *Int.* 1076 *J. Quantum Chem.* **2000**, *80*, 1107–1115.
- 1077 (12) Tratnyek, P. G.; Hoigne, J. Oxidation of substituted phenols in the environment: a QSAR analysis of rate constants for reaction with singlet oxygen. *Environ. Sci. Technol.* **1991**, *25*, 1596–1604.
- 1079 (13) Canonica, S.; Hellrung, B.; Wirz, J. Oxidation of phenols by triplet aromatic ketones in aqueous solution. *The Journal of Physical Chemistry A* **2000**, *104*, 1226–1232.
- 1081 (14) D'Auria, M. The Paternò-Büchi reaction a comprehensive review. *Photochem Photobiol Sci* **2019**, *18*, 2297–2362.
- 1083 (15) Fréneau, M.; Hoffmann, N. The Paternò-Büchi reaction—Mechanisms and application to organic synthesis. *J. Photochem. Photobiol. C* **2017**, *33*, 83–108.
- 1085 (16) Gersdorf, J.; Mattay, J.; Goerner, H. Radical cations. 3. Photoreactions of biacetyl, benzophenone, and benzil with electron-rich alkenes. *J. Am. Chem. Soc.* **1987**, *109*, 1203–1209.

- 1087 (17) Eckert, G.; Goez, M. Photoinduced Electron-Transfer Reactions of Aryl Olefins. 1. Investigation of the Paterno-Buechi Reaction between Quinones and Anetholes in Polar Solvents. *J. Am. Chem.* Soc. **1994**, 116, 11999–12009.
- 1090 (18) Smith, J. D.; Kinney, H.; Anastasio, C. Aqueous benzene-diols react with an organic triplet excited state and hydroxyl radical to form secondary organic aerosol. *Phys. Chem. Chem. Phys.* 1092 **2015**, *17*, 10227–10237.
- 1093 (19) Ma, L.; Guzman, C.; Niedek, C.; Tran, T.; Zhang, Q.; Anastasio, C. Kinetics and mass yields of aqueous secondary organic aerosol from highly substituted phenols reacting with a triplet excited state. *Environ. Sci. Technol.* **2021**, *55*, 5772–5781.
- 1096 (20) Smith, J. D.; Sio, V.; Yu, L.; Zhang, Q.; Anastasio, C. Secondary organic aerosol production from aqueous reactions of atmospheric phenols with an organic triplet excited state. *Environ. Sci.* 1098 *Technol.* **2014**, *48*, 1049–1057.
- 1099 (21) Rayner, D. M.; Wyatt, P. A. H. Laser study of the protonation equilibrium of triplet benzophenone. *J. Chem. Soc., Faraday Trans. 2* **1974**, *70*, 945.
- 1101 (22) Appiani, E.; Ossola, R.; Latch, D. E.; Erickson, P. R.; McNeill, K. Aqueous singlet oxygen 1102 reaction kinetics of furfuryl alcohol: effect of temperature, pH, and salt content. *Environ. Sci.*: 1103 *Processes Impacts* **2017**, *19*, 507–516.
- 1104 (23) Kochany, J.; Bolton, J. R. Mechanism of photodegradation of aqueous organic pollutants. 2.

  1105 Measurement of the primary rate constants for reaction of hydroxyl radicals with benzene and some halobenzenes using an EPR spin-trapping method following the photolysis of hydrogen peroxide. *Environ. Sci. Technol.* 1992, 26, 262–265.
- 1108 (24) Felber, T.; Schaefer, T.; He, L.; Herrmann, H. Aromatic carbonyl and nitro compounds as photosensitizers and their photophysical properties in the tropospheric aqueous phase. *J. Phys.* 1110 *Chem. A* **2021**, *125*, 5078–5095.
- Walpen, N.; Houska, J.; Salhi, E.; Sander, M.; von Gunten, U. Quantification of the electron donating capacity and UV absorbance of dissolved organic matter during ozonation of secondary wastewater effluent by an assay and an automated analyzer. *Water Res.* **2020**, *185*, 116235.
- 1114 (26) Yuan, Y.; Zhang, H.; Wei, Y.; Si, Y.; Li, G.; Zhang, F. Onsite quantifying electron donating capacity of dissolved organic matter. *Sci. Total Environ.* **2019**, *662*, 57–64.
- Wang, D.; Bolton, J. R.; Hofmann, R. Medium pressure UV combined with chlorine advanced oxidation for trichloroethylene destruction in a model water. *Water Res.* **2012**, *46*, 4677–4686.
- 1118 (28) Walpen, N.; Schroth, M. H.; Sander, M. Quantification of Phenolic Antioxidant Moieties in
   1119 Dissolved Organic Matter by Flow-Injection Analysis with Electrochemical Detection. *Environ.* 1120 Sci. Technol. 2016, 50, 6423–6432.
- 1121 (29) Kaur, R.; Labins, J. R.; Helbock, S. S.; Jiang, W.; Bein, K. J.; Zhang, Q.; Anastasio, C.
  1122 Photooxidants from brown carbon and other chromophores in illuminated particle extracts. *Atmos. Chem. Phys.* **2019**, *19*, 6579–6594.